CHALMERS
UNIVERSITY OF TECHNOLOGY

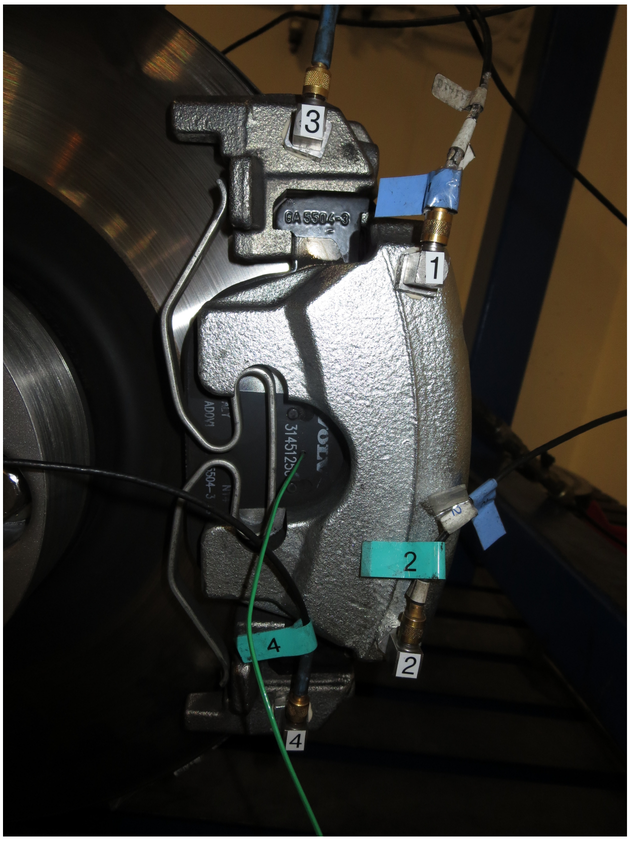

Development of Multi-body Model to Simulate Creep Groan in ADAMS

Friction regularization approach

Master's thesis in Master Programme Sound and Vibration

NICKLAS FRANSSON

Department of Civil and Environmental Engineering
CHALMERS UNIVERSITY OF TECHNOLOGY
Gothenburg, Sweden 2016

MASTER'S THESIS 2016:BOMX02-16-102

Development of Multi-body Model to Simulate Creep Groan in ADAMS

Friction regularization approach

NICKLAS FRANSSON

Department of Civil and Environmental Engineering
Division of Applied Acoustics
Vibroacoustics Group
CHALMERS UNIVERSITY OF TECHNOLOGY
Gothenburg, Sweden 2016

Development of Multi-body Model to Simulate Creep Groan in ADAMS
Friction regularization approach
NICKLAS FRANSSON

Supervisor:	Bart de Korte	*Volvo Cars Corporation*
Examiner:	Patrik Höstmad	*Chalmers University of Technology*

Master's Thesis 2016:BOMX02-16-102
Department of Civil and Environmental Engineering
Division of Applied Acoustics
Vibroacoustics Group
Chalmers University of Technology
SE-412 96 Gothenburg
Telephone +46 31 772 1000

Cover: Close-up photograph of brake system rig as used in the experimental measurements of creep groan.

Typeset in LaTeX
Gothenburg, Sweden 2016

Development of Multi-body Model to Simulate Creep Groan in ADAMS
Master's thesis in Master Programme Sound and Vibration
NICKLAS FRANSSON
Department of Applied Acoustics
Chalmers University of Technology

Abstract

Creep groan is a friction induced, low frequency instability problem that occurs in automotive brakes at low speeds, such as when the car is moving from, or to a complete stop. The vibration that is generated at the disc interface pollutes the car's interior and exterior space with unwanted noise that can be correlated with customer dissatisfaction and attrition. To this end, this thesis is involved with developing a computer model for accurate simulations of creep groan, by the prospect of virtual testing and brake NVH verification. Creep groan measurements were conducted on an experimental brake system rig in a laboratory environment which in addition to vibration behaviour, also allowed for the retrieval of various operation parameters. A multi-body model was then developed in ADAMS software using rigid and flexible geometries. A regularized friction description is used to model the contact dynamics. From analysing numeric and analytic solutions it could be demonstrated that the computer models predictions were largely consistent with the measured vibrations in terms of stick-slip, excited modes and overall spectral content.

Keywords: Automotive brake NVH, creep groan, stick-slip instability, ADAMS modelling, friction regularization, numerical integration

Acknowledgements

The project was carried out at the R&D department of Volvo Cars Corporation in Torslanda; a workplace that harbours much knowledge and generosity. I am grateful toward all who have helped me on site with everything from practical to administrative matters.

I would like to thank my supervisor Bart de Korte and my examiner Patrik Höstmad. A special thanks goes out to Patrick Sabiniarz who, despite not being formally involved with the thesis project, has been an invaluable asset and source for knowledge.

Nicklas Fransson, Gothenburg, June 2016

Contents

List of Figures

List of Tables

1
Introduction

Over the past decades, problems involving noise and vibration generated from the brake system has become recognised as a steadily growing concern in the automotive industry. These issues do not necessarily regard to vehicle safety, but of the cost associated with customer complaints and warranty claims emanating from inadequate acoustic comfort and over-all driving impression. From a study in 2001, it was suggested that warranty claims in the brake NVH category generates annual costs of up to $1 billion US dollars[3] in North America alone. And today, given the rising sales in automotives and ever-increasing customer expectations; warranty related costs can be expected to be higher than ever to manufacturers.

The brake system is a critical component to a vehicles safety and performance. Take in consideration its immediate component parts are numerous, the range of braking conditions under which it operates and the large amounts of energy that transmits on account of friction upon braking. It's not difficult to understand that, in effect, the brake become a kaleidoscope of sound and vibroacoustic phenomena. Conceding that it's impossible to categorise all sounds that may be produced, there are some noise and vibration occurrences that are especially annoying and frequenting in brake systems. These are the collectively labeled brake noises, all of which associated with some unique triggering mechanism and/or psychoacoustic characteristic.

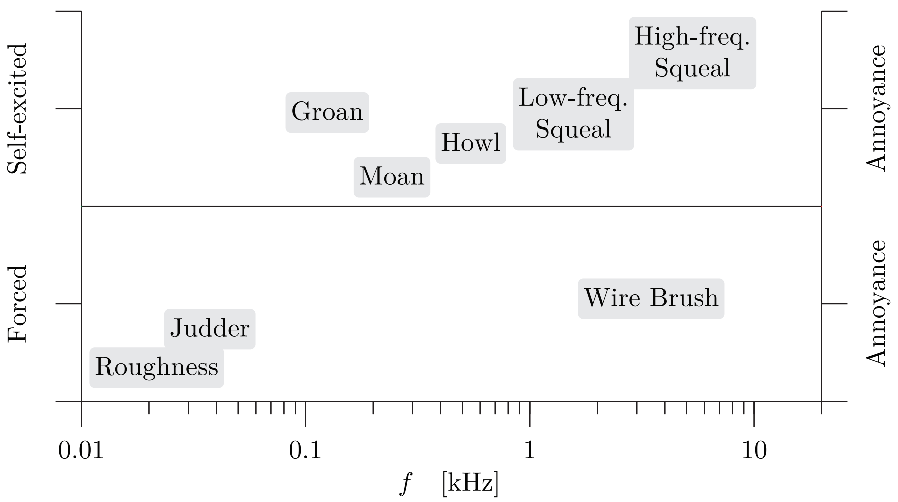

Figure 1.1: Brake noises by triggering mechanism and approx. annoyance rating.

1.1 Purpose and background

NVH verification of brakes have traditionally been based on physical prototyping, however, today at VCC there is a strong drive to increase the virtual verification capability for the brake functions in order to shorten the development time and cost. In that spirit, this thesis is concerned with modelling creep groan, which is a particular low frequency instability phenomenon occurring in automotive brakes.

Creep groan generally occurs as the brakes are activated and the vehicle is driving at low speeds, such as when moving from, or to a complete stop. It involves stick-slip phenomenon at the pad/disc interface and the resulting noise and vibration highly influences the driver's quality perception of the vehicle. Optimizing brake and suspension designs to eliminate creep groan has been a persistent problem to NVH engineers: Though some control factors have been identified, no non-interfering and/or definitive design solutions have been found to date.

1.2 Aim

The aim of the project can be condensed to three main parts:

1. Design a experiment that produce creep groan in a lab environment

2. Develop a computer model to simulate the experiment

3. Validate and calibrate the simulations toward the experiment results

1.3 Limitations and assumptions

To gain accurate predictions by means of computer modelling and simulation requires a large body of experimental data. Beyond measuring the vibrations upon operation, there is a need to know various parameters that assisted to generate these particular vibrations (as to reduce time spent on calibration and avoid guess-work). In the main experiment for this thesis, some of these parameters could be obtained directly using transducers, such as measuring instantaneous braking pressure, while others are much more complex to obtain experimentally, given the equipments at hand, time constraints, etc. And so, for some input parameters there is a need for using nominal, calculated or estimated values when creating simulations. This mainly concern operation values of bushings and the contact interface.

The other important aspect are the approaches on how to implement these values into the computer model. For the purpose of this thesis, one assumption is that damping does not need to be modelled with a frequency dependence given the low frequency nature of creep groan. As for contact dynamics, Amonton's laws of dry friction with a regularization approach is used. The friction model will not include a nonholonomic constraints for regime transitions.

1.4 Outline of the report

The report provides a near-chronological narration of the entire project from start to finish. The theory in Chapter 2 is committed to creep groan, leaving other theoretical notions related with modelling, analysis, etc., to be introduced throughout the report. Chapter 3 focuses on the implementation and functions of the experimental rig while Chapter 4 display and analyse the results produced from the measurements. The chapters 4 and 5 are related to the model development and simulation evaluation.

2

Friction-vibration interaction

For all dynamic mechanical systems, vibrations are developed between sliding surfaces by account of friction. The physical aspects of friction cover a wide range of lengths and time scale[3]. At the microscopic level, friction acts to transfer kinetic energy to thermal energy through subatomic interaction. On the other hand, at macroscopic level, friction imposed on one subsystem will act to translate kinetic energy and set other neighbouring bodies to motion.

For particular setups, the friction and the vibration it develop interacts and create feedback loops that trigger oscillations in various unsteady and non-ergodic manners. That is friction-vibration interaction, or, friction-excited vibrations, and an array of acoustic phenomena are postulated to arise on this basis, including creep groan. Additional examples are snow squelching underfoot, whiteboards squeaking, creaking door hinges, brake squeal, rail-wheel noises and earthquakes[3],[11].

2.1 Theoretical background

The main concepts underlying creep groan are introduced in this section.

2.1.1 Friction and contact dynamics

Friction is a resistance force that act on an object as it slides along a surface or move through a fluid. The friction coefficient, μ, is a dimensionless scalar that describes a relation between two perpendicular forces

$$\mu = \frac{F_\mathrm{f}}{F_\mathrm{n}}, \tag{2.1}$$

where F_n is the normal force, and F_f is the resulting friction force. The friction coefficient at an interface is subject to change on account of an array of properties that may vary over time, including, but not limited to: relative velocity, humidity, temperature, deformation, and wear[15],[9]. An axiomatic derivation of friction is thus impractical; all-encompassing analytical friction models do not exist and in lieu of which, available friction models are established by phenomenological, or empirical means[7]. In the following, we are considering a reduced friction model based on Amontons' laws of dry friction[4],[8] with a dependency on relative velocity:

1. The force of friction is directly proportional to the applied load. (Amontons' 1st Law)

2. The force of friction is independent of the apparent area of contact. (Amontons' 2nd Law)

3. Kinetic friction is independent of the sliding velocity. (Coulomb's Law)

It should be stressed how these laws only handle a narrow perspective of the extremely complicated nature of interface friction. They are constructs, helpful by their approximation and simplicity in a limited range of conditions. For example, in cases where adhesion is significant (*e.g.*, sticky-tape, car tyres, etc.), Amontons 2nd law fails as contact area cannot be neglected.

On the topic of friction-vibration interaction, mainly two approaches are used for modelling friction in literature. They are the *regularization approach*[1] and the *non-smooth approach*. These approaches offer different ways of mathematically describing the discontinuities of friction regimes and come with different strengths and weaknesses.

A regularized friction law writes friction as a smooth function of relative velocity (v_{rel}), which allows for expressing the dynamic system in terms of some ordinary differential equation (ODE). However, solving the resulting differential equation analytically is not possible because of nonlinearities in friction forces, and calculating the motion numerically is computationally ineffective as it requires integration of extremely small timescale as owed by the ODE being stiff (numerically unstable). The qualitative downsides with regularizing friction is that position and velocities are smooth and in turn produce small, false, oscillations that may cause initial value problems for larger systems. Formulating and choosing parameters that express the regularization also bring uncertainty as it can be written in multiple forms, for example[6]

$$\mu(v_{\text{rel}}) = \mu_{\text{k}} \left[1 - e^{-\beta|\epsilon|v_{rel}}(1 + \left(\frac{\mu_{\text{s}}}{\mu_{\text{k}}} - 1 \right) e^{-\alpha|\epsilon v_{\text{rel}}|}) \right] \text{sgn}(\epsilon v_{\text{rel}}), \tag{2.2}$$

where f_{r} is the friction regime ratio $\mu_{\text{s}}/\mu_{\text{k}}$ and β, α, ϵ are parameters related to the rate of change. Another potential form could be[13]

$$\mu(v_{\text{rel}}) = \alpha_1 e^{\alpha_2 v_{\text{rel}}^2} + \alpha_3 v_{\text{rel}} + \alpha_4, \tag{2.3}$$

where α_1-α_4 are parameters to describe the friction curve. On the other hand, regularizing friction is straight-forward and easy to implement, and can be advantageous in cases where computation is not an issue (see further below). Furthermore, as these systems can be expressed as a single ODE, it allows for linearization of friction curve and 'interpretative' complex eigenvalue analysis to study possible instabilities.

The switch approach writes the friction regimes as independent sets, meaning the system is instead described by multiple non-stiff ODE's which can reduce calculation cost significantly[14].

$$\mu(v_{rel}) = \begin{cases} \mu_{\text{k}} & \text{for } v_{rel} > 0 \\ \mu_{\text{s}} & \text{for } v_{rel} = 0^+ \\ -\mu_{\text{s}} & \text{for } v_{rel} = 0^- \\ -\mu_{\text{k}} & \text{for } v_{rel} < 0 \end{cases} \tag{2.4}$$

[1] Otherwise known as smooth or normalization approach.

Friction in Equation 2.4 changes at infinitesimal scale resulting in non-smooth changes in forces and velocities. However such behaviour has been proven physically inaccurate; mechanical contact with a distributed mass and compliance cannot instantaneously change its force vector[5].

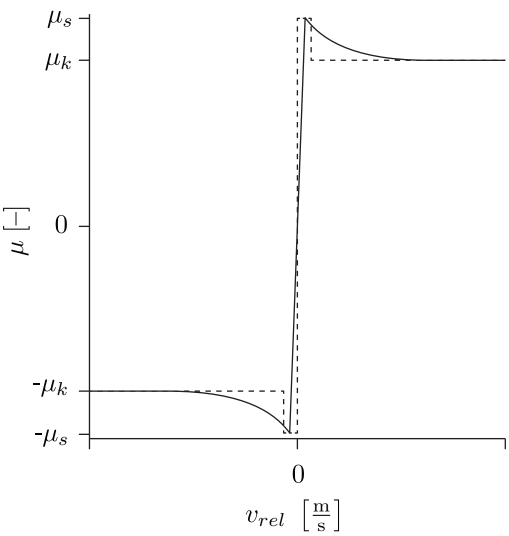

Figure 2.1: Friction as a function of relative velocity with the regularized friction law (——) and the non-smooth friction law (- - -).

These friction models are further covered and compared in *Stick-Slip Vibrations Induced by Alternate Friction Models* by R.I. Leine et al[14].

2.1.2 Friction regime effect on vibration

For friction profiles with a declining relation between static and kinetic friction regime, the 'parent' bodies holds a property akin to negative damping. Negative damping can be described as an unbalanced mechanism where potential energy is accumulated in one regime and released into another less constrained regime[2]. By this manner, a basis for sustained self-excitation and instability is created for continuous systems. The described phenomenon is called stick-slip and make for quasi-harmonic and sometimes chaotic vibration, it is recognized by sawtooth patterns in time–displacement plots[11].

The occurrence of such instability in a system with respect to friction necessitates negative damping, however it does not ensure it. While several different conditions exist, the most direct and easily understood condition for instability is found by comparing damping to negative damping:

$$\begin{cases} \gamma - \dfrac{d\mu_{s\to k}}{dv_{\mathrm{rel}}} F_{\mathrm{n}} < 0 \quad \Rightarrow \text{ Instability} \\ \gamma - \dfrac{d\mu_{s\to k}}{dv_{\mathrm{rel}}} F_{\mathrm{n}} > 0 \quad \Rightarrow \text{ Stability} \end{cases} \tag{2.5}$$

[2]Negative damping can only be mathematically evaluated for smooth friction models and is a strictly heuristic concept; it does not create vibration from heat.

where $[d\mu_{\mathrm{s}\to\mathrm{k}}/dv_{\mathrm{rel}}]F_{\mathrm{n}}$ is the linearized friction force at an interface (for some v_{rel} in the stick-to-slip transition) and γ represent the damping at the interface.

2.2 Mathematical modelling

As an effort in gaining insight of creep groan vibrations, this section offer physical interpretations and mathematical modelling of a brake system. For convenience in regards to calculation and transparency, the system is simplified and represented on reduced order(s). In doing so, we may formulate preliminary assumptions and weighting of brake system parameters with regard to instability. The first part of this investigation focuses mainly on understanding stick-slip itself while the second part introduces further conditions to simulate creep groan.

2.2.1 Friction in SDOF systems

The simplistic model for which stick-slip vibrations can be studied is presented here. Consider a body with mass, m, riding on a belt that moves at a prescribed velocity, v. The body is attached to inertial space by a spring, k, and loaded onto the belt by a normal force, N.

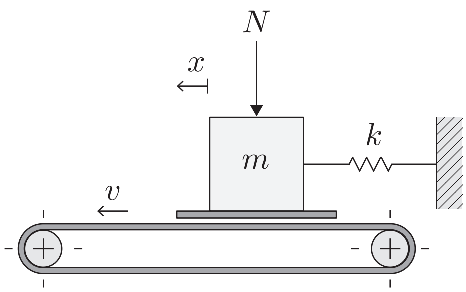

Figure 2.2: SDOF model

Acceleration by gravity as well as damping is ignored and we are only interested in the forces acting in the horizontal direction, designated x.

Studying Figure 2.2, the spring force increases over distance from its relaxed position as $F_\mathrm{k} = kx$. From Newton's second law, the inertial force of the mass is $F_\mathrm{a} = m\,[d^2x/dt^2]$. Applied with equation (2.2), the friction force is $F_\mathrm{f} = \mu(v_\mathrm{rel})N$, where $v_\mathrm{rel} = v - dx/dt$ is the surface velocity between slider and belt and μ is formulated by Equation (2.2).

By separation of forces we find $F_f = F_k + F_a$, and so the state equation governing this system reads

$$0 = kx - \mu(v_{rel})N + m\frac{d^2x}{dt^2}. \tag{2.6}$$

From Equation (2.6) and Figure 7.2 we can observe that the system is nonlinear due to frictions dependence on relative velocity. By the onset of relative movement $v_\mathrm{rel} = 0 \rightarrow v_\mathrm{rel} \neq 0$ the friction force declines in accordance to our friction model, creating what can be described as negative damping. The occurrence of instability is thus directly related to the difference and rate between friction regimes as implied by equation (2.5). The system motion is found numerically with MATLAB software using build-in stiff ODE-solver `ode15s` for boundary conditions

$$\begin{bmatrix} x(t=0) \\ \left.\dfrac{dx}{dt}\right|_{t=0} \end{bmatrix} = \begin{bmatrix} 0 \\ v \end{bmatrix}. \tag{2.7}$$

Here we may study the effect of different friction parametrizations. In *Case A* the friction is dependent on relative velocity, whereas in *Case B* the friction is constant, otherwise their parameters are identical with $v = 1$ m/s, $m = 2$ kg, $k = 10$ kN/m and $N = 10$ kN.

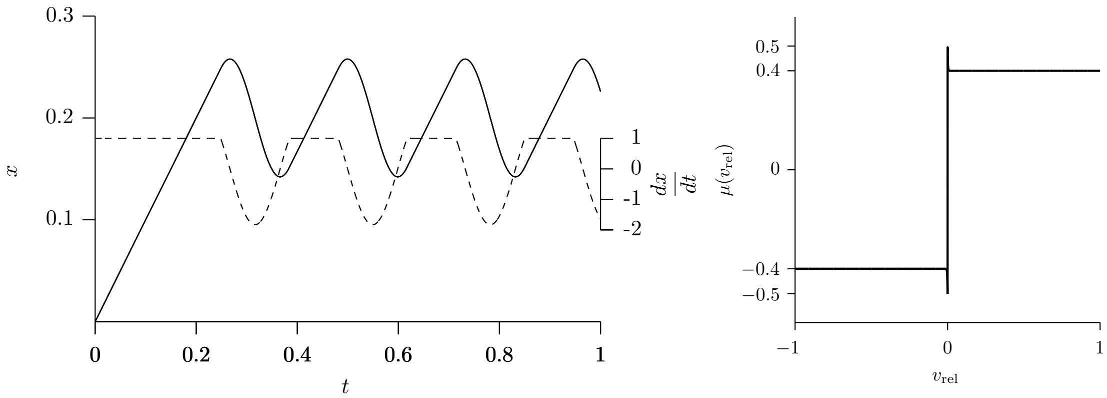

(a) *Case A*

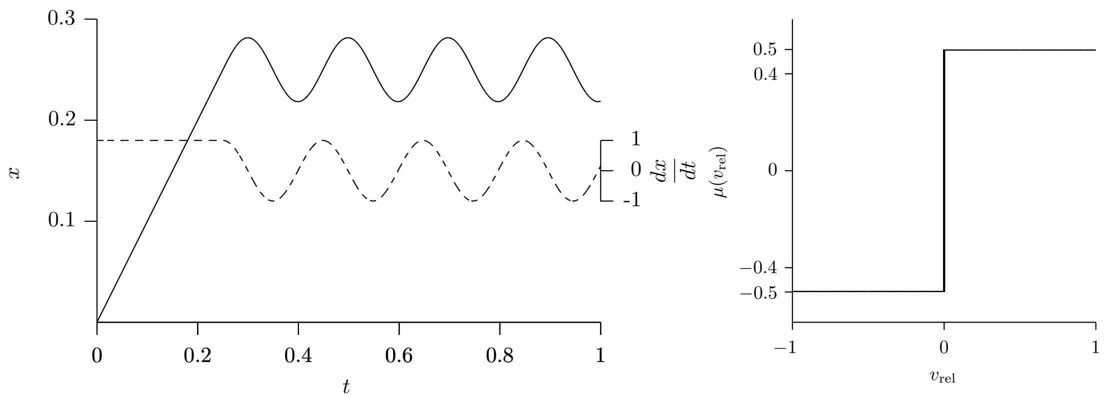

(b) *Case B*

Figure 2.3: Mass displacement (——), mass velocity (- - -) histories to the left and friction as a function of relative velocity to the right.

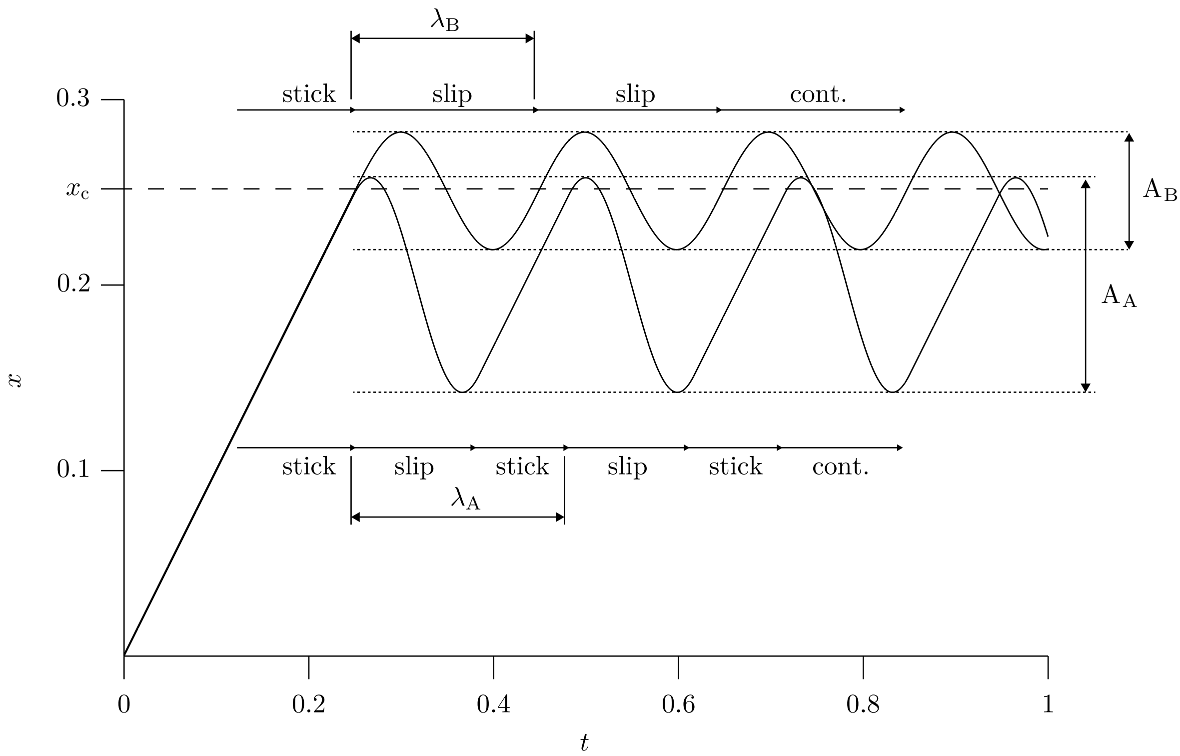

Figure 2.4: Displacement over time for both cases with descriptions of states, amplitudes and wavelengths.

For the initial phase of both cases, the mass sticks to and ride with the belt with at a constant velocity of v as $F_f > F_k$. Then, as the system approaches critical displacement $F_f \approx F_k$, the mass lapses into slip ($v_{rel} \neq 0$) and the differences appear.

For case A the friction coefficient drops from 0.5 to 0.4, meaning its effective critical displacement is lowered, and thus it will rebound quickly. Stick between mass and belt is then recovered and the process can repeat. For case B, friction remains constant under $v_{rel} \neq 0$, the system can be seen to instead steadily oscillate around the critical displacement by account of its initial inertia.

2.2.2 Friction in MDOF systems

While the genesis of creep groan can be demonstrated with a SDOF model, additional freedoms needs to be introduced for further approximate dynamics. From a qualitative standpoint, numerical solutions to MDOF systems goes a long way for analysing creep groan, and similar models presented in this section has been explored in the past by G. Chen[11], A.R. Crowther el al.[1], etc.

In Figure 2.5, a translational representation of a vehicle brake system is illustrated[3]. The setup includes masses for transmission (m_1), disc (m_2) and brake (m_3). The transmission and disc are coupled via the drive-axle (k_1, c_1) while the brake and chassi is coupled via the suspension (k_2, c_2). Again, the friction between disc and brake is described with Equation (2.2).

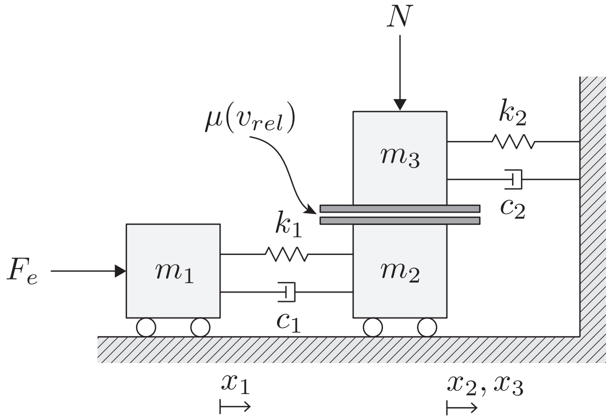

Figure 2.5: Translatory 3-DOF representation of the drivetrain.

Expanding on the same concepts as presented in section 2.2.1, but for multiple masses and now also introducing viscous damping forces between masses, the equation of motion (established in Appendix A) for the system in Figure 2.5 can be written as

$$\begin{bmatrix} -F_e \\ \mu(v_{rel})N \\ -\mu(v_{rel})N \end{bmatrix} = \begin{bmatrix} -k_1 & k_1 & 0 \\ k_1 & -k_1 & 0 \\ 0 & 0 & -k_3 \end{bmatrix} \begin{bmatrix} x_1 \\ x_2 \\ x_3 \end{bmatrix} + \begin{bmatrix} -c_1 & c_1 & 0 \\ c_1 & -c_1 & 0 \\ 0 & 0 & -c_3 \end{bmatrix} \begin{bmatrix} \dot{x}_1 \\ \dot{x}_2 \\ \dot{x}_3 \end{bmatrix} + \dots$$
$$\dots + \begin{bmatrix} -m_1 & 0 & 0 \\ 0 & -m_2 & 0 \\ 0 & 0 & -m_3 \end{bmatrix} \begin{bmatrix} \ddot{x}_1 \\ \ddot{x}_2 \\ \ddot{x}_3 \end{bmatrix} \tag{2.8}$$

where $v_{rel} = \dot{x}_2 - \dot{x}_3$ and the regularization parametrization is the same as for SDOF case A. The motion of this system is again numerically integrated using MATLAB software (see Appendix B) and the simulation result for some arbitrary system parameters can be found in Figure 2.6.

[3]If necessary, the rotatory disc and transmission position, inertia, etc. can be reformulated as translational using $M_i = J_i/r_e^2$ and $\dot{x} = r_e, \dot{\Theta}$.

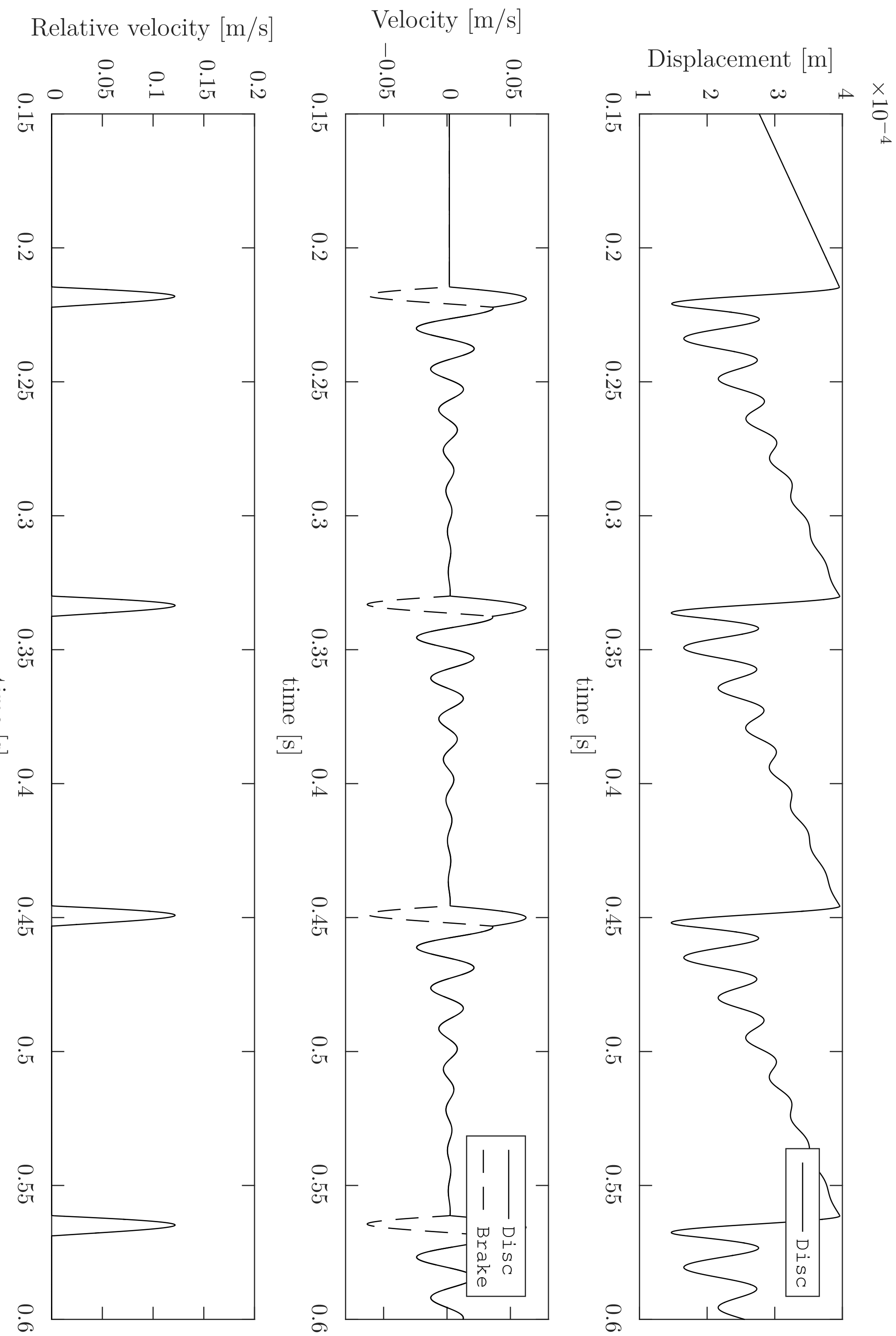

Figure 2.6: Simulation results for $\dot{x}_1 = 5 \times 10^{-3}$ m/s, $k_1 = 1.4 \times 10^{6}$ N/m, $k_2 = 2500000$ N/m, $d_1 = 1.46 \times 10^{3}$ Ns/m, $d_2 = 250$ Ns/m, $m_2 = 13$ kg, $m_3 = 9.8$ kg

Note that, by account of friction coupling the system will now contain different mode sets depending on stick or slip: *I.e.*, as stick occurs, m_3 and m_2 are effectively one combined mass whereas for slip they can have separate vibrations.

Formulating precise descriptions on parameters effect on behaviour for this kind of unstable system is problematic, as between some parameter changes the system can undergo abrupt vibrational transitions or simply start to behave chaotically[11]. However, it is still possible to gain a general understanding inside some vibrational regime with a parametric study, by for example modifying 'suspension' stiffness (k_2) and damping (d_2) values as performed in Figure 2.6.

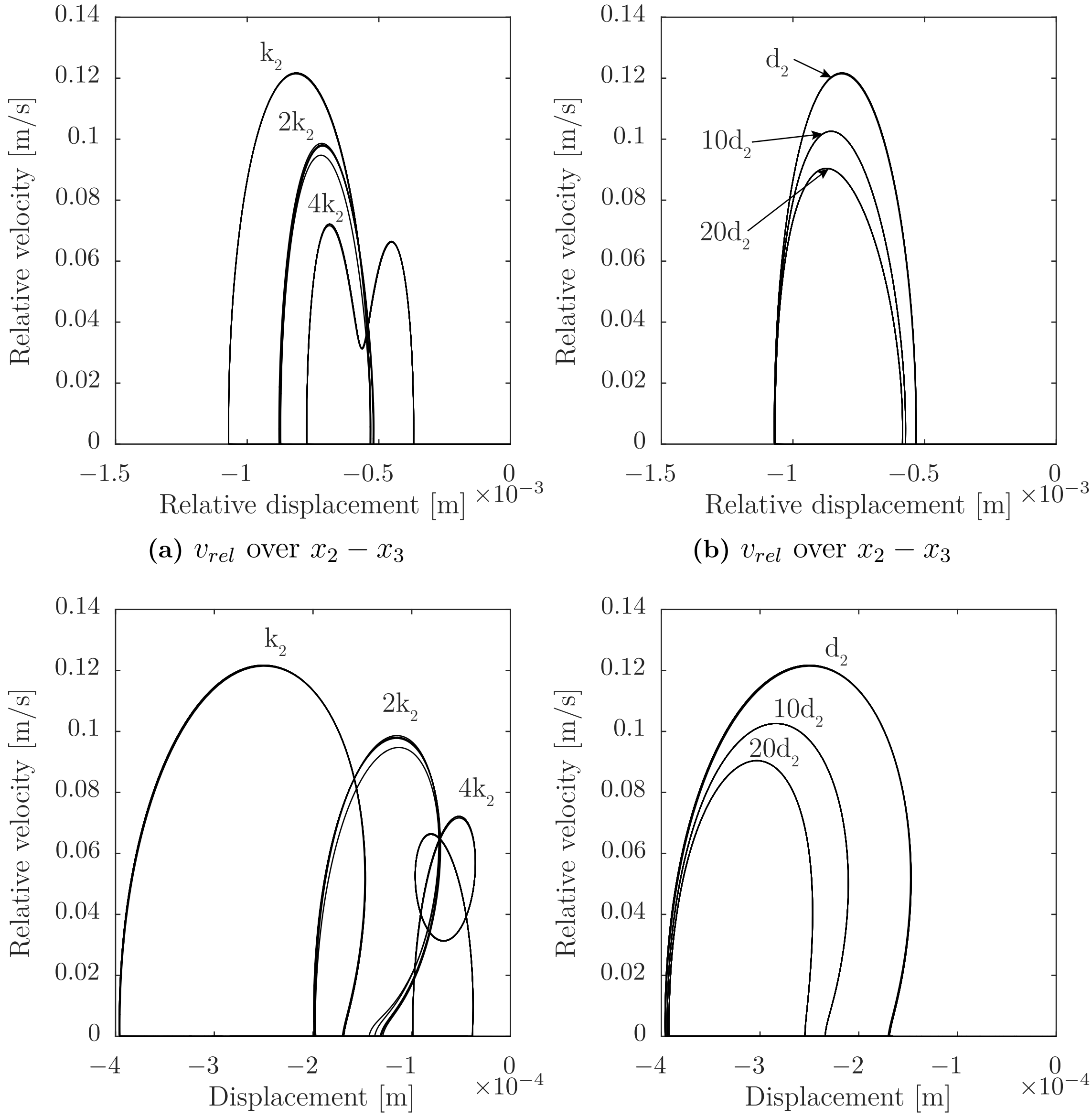

(a) v_{rel} over $x_2 - x_3$

(b) v_{rel} over $x_2 - x_3$

(c) v_{rel} over x_3

(d) v_{rel} over x_3

Figure 2.7: Phase plots showing parameter effects on stick-slip vibration.

With Figure 2.7 it is demonstrated that from an increase in damping or stiffness the slip amplitude will decrease. However, note that the decrease in amplitudes occurs on different basis as for a stiffness increase the stick-to-slip transition is accelerated whereas for damping the slip-to-stick transition is accelerated.

In figures 2.7 (a,c) an abrupt qualitative change in dynamics occurs from $2k_2 \rightarrow 4k_2$. The transition is the result of a stick not being gained until m_3 has completed one slip rotation. This manner of system branching to oscillatory states as displayed in previous figures is called *Hopf bifurcation* and is caused by eigenvalues crossing the complex plane imaginary axis.

Brief note on linearization

By linearizing the friction force ($e.g.$, $[d\mu_{\mathrm{s}\rightarrow\mathrm{k}}/dv_{\mathrm{rel}}]N$) in Equation (2.8) the system lends itself as the linear homogeneous differential equation

$$\mathbf{M}\frac{d^2\boldsymbol{x}}{dt^2} + [\mathbf{C} - \mathbf{F}_\mathbf{f}]\frac{d\boldsymbol{x}}{dt} + \mathbf{K}\boldsymbol{x} = 0 \tag{2.9}$$

of which the eigenvalues and eigenvectors can be found by $(\mathbf{M}\lambda^2 + [\mathbf{C} - \mathbf{F}_\mathbf{f}]\lambda + \mathbf{K})\boldsymbol{X} = 0$ using MATLAB's QEP solver `[X,EIG] = polyeig(K,C-Ff,M)`. Among other things, this allows for visualizing the instabilities and occurring vibrations with respect to some parameter.

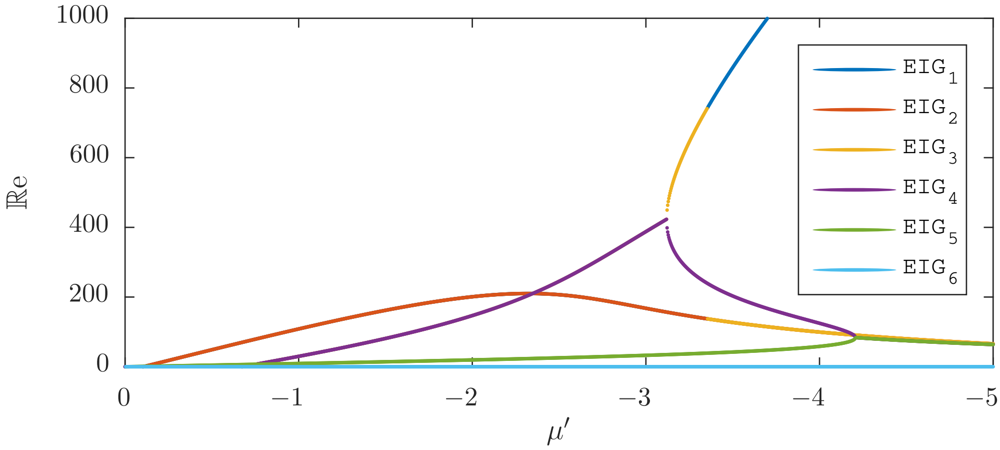

(a) Real

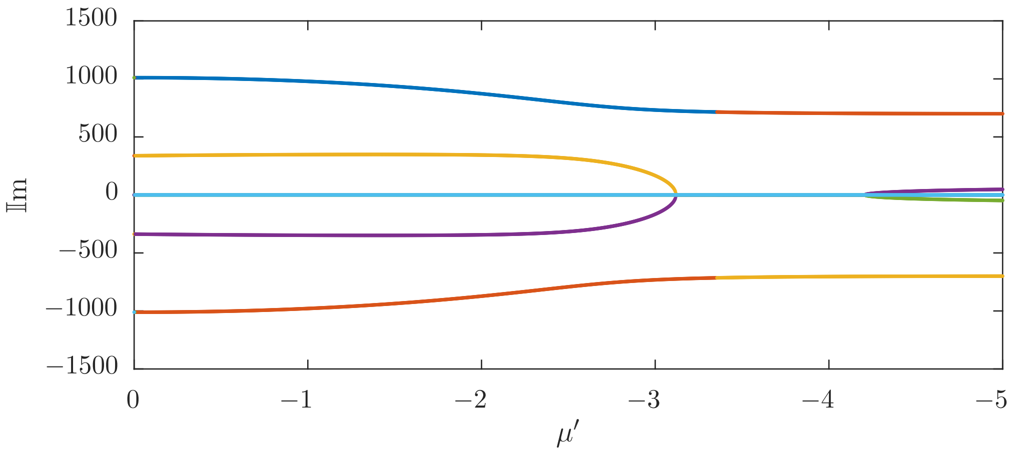

(b) Imaginary

Figure 2.8: Complex eigenvalue of system

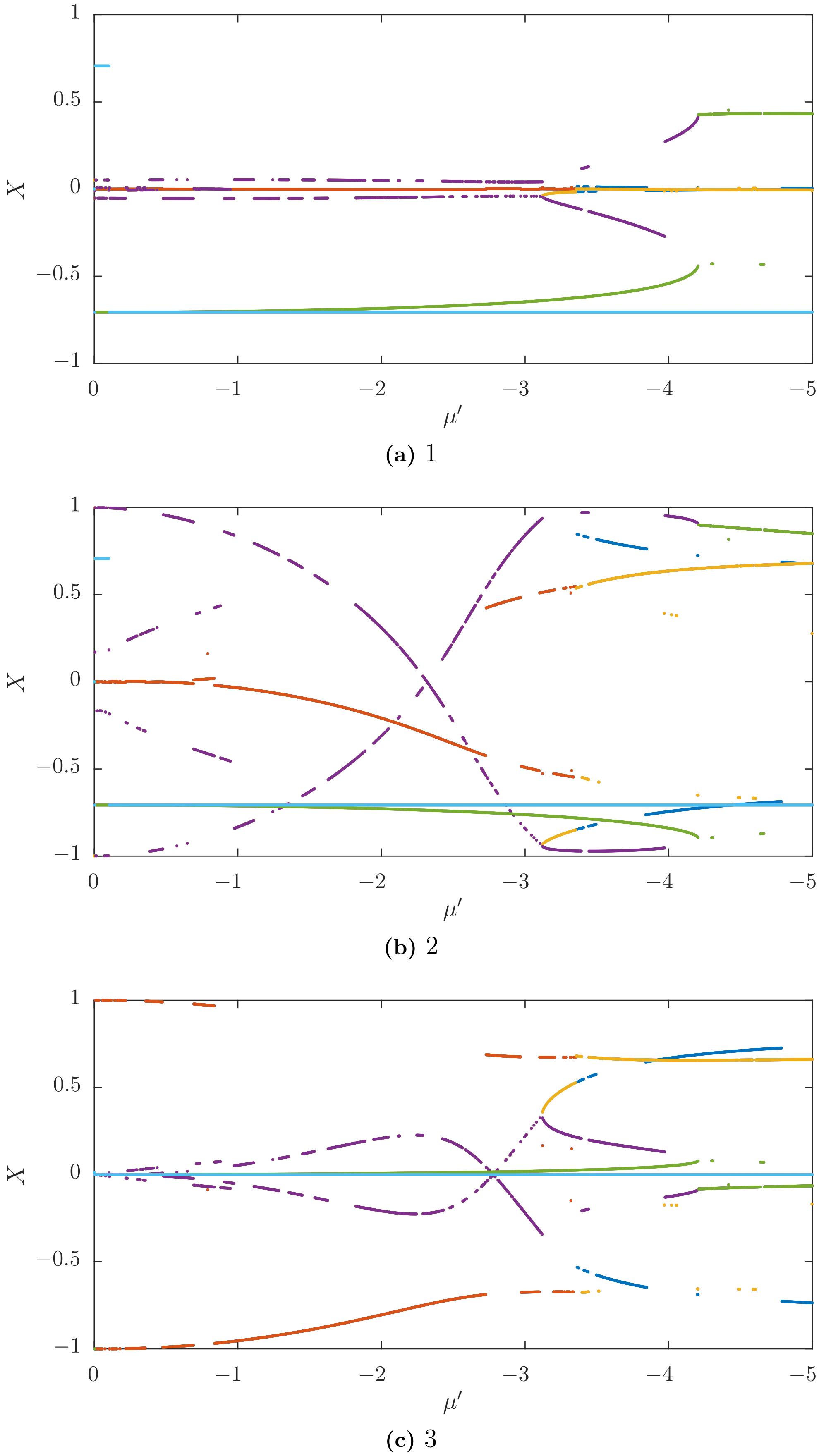

Figure 2.9: Bifurcation maps of the subsystems.

3
Measurements

Experimental measurements of a creep groan rig are taken in a laboratory environment at VCC, with the intention of achieving accurate data for CAE model design and its validation.

3.1 Creep groan

The rig setup includes a functioning brake system with suspension, mounted onto a rigid steel frame by the suspension upper strut and control arm bushings. The frame is in turn fastened onto a heavy steel beam table with four clamps. A linear hydraulic cylinder animates the brake disc via wire whereby attaching it on the disc's tangent, the wire coils and rides along the perimeter, generating equal torque over angular displacement. As opposed to a driveshaft that only produces torque, the brake system in the experiment is subjected to a lateral force.

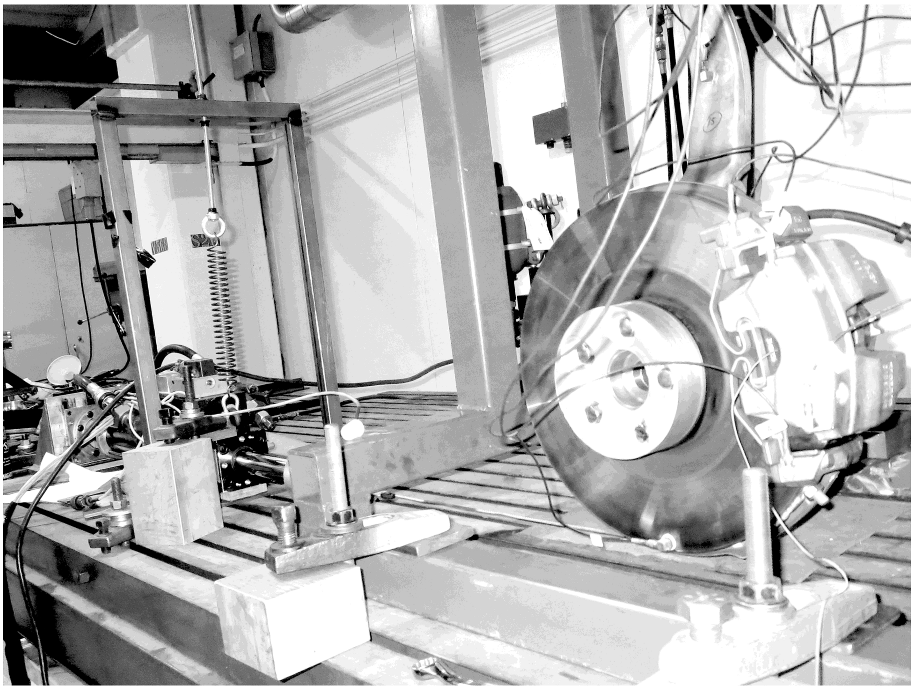

Figure 3.1: Photo of the rig showing the brake system etc. (to the right) and hydraulic cylinder (to the left).

The rig is devised to operate under various controlled conditions as to make sure creep groan is achieved. Adjustable parameters include braking pressure and contraction speed of the hydraulic cylinder where the former is controlled manually by screwing a pin into the brake pipe and the latter is controlled by programming the hydraulic cylinder.

A ceramic glue layer was used to attach 9 triaxial accelerometers at various positions of the brake, disc and suspension (see Table 3.1). The accelerometers, except for the one attached to the disc, are placed pairwise on various components.

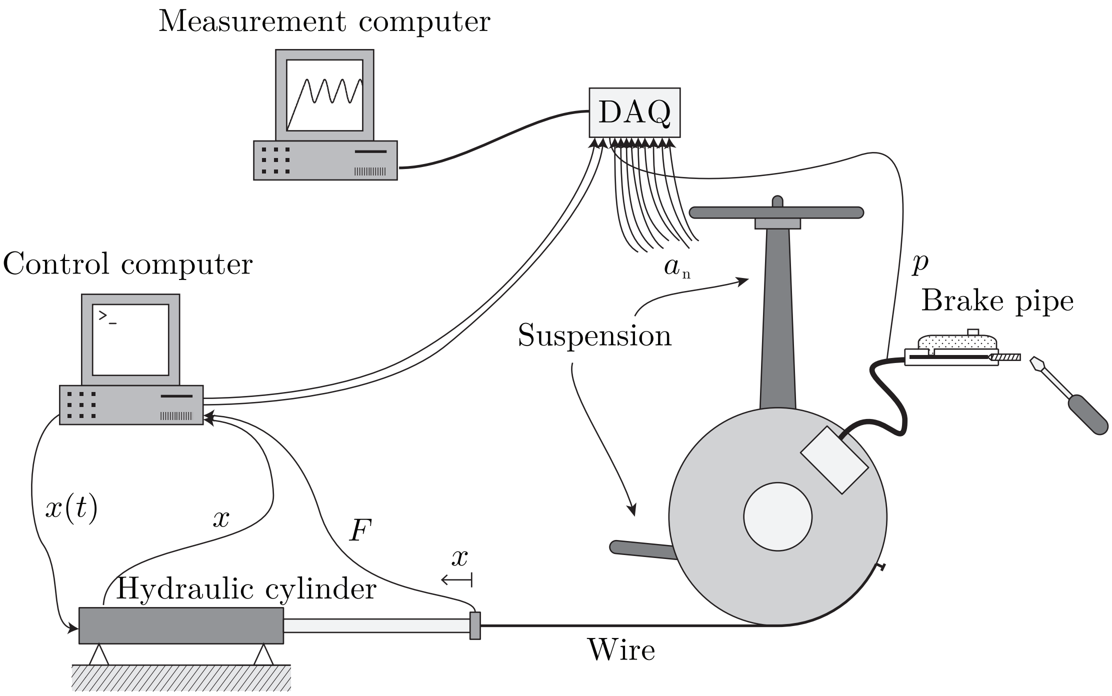

Figure 3.2: Basic illustration of rig and variable control mechanisms.

Table 3.1: Measurement transducers

Class	Transducer ($PQ_{\#}$)	Signal	Placement
AC coupled	Accelerometer (a_1)	1–3	Caliper top
	Accelerometer (a_2)	4–6	Caliper bottom
	Accelerometer (a_3)	7–9	Carrier top
	Accelerometer (a_4)	10–12	Carrier bottom
	Accelerometer (a_5)	13–15	Knuckle top
	Accelerometer (a_6)	16-18	Knuckle bottom
	Accelerometer (a_7)	19-21	UCA ball joint
	Accelerometer (a_8)	22-24	UCA arm
	Accelerometer (a_9)	25-27	Disc edge
DC coupled	Load cell (p)	28	Brake pipe/cylinder
	Load cell (F)	29	Hydraulic cylinder rod
	Position sensor (x)	30	Hydraulic cylinder rod

3.2 Wire

A complimentary measurement was setup to calculate the properties of the wire used in the rig through frequency response functions. As seen in see Figure 3.3, a mass of 10 kg is suspended by the wire to a stiff beam, such as to conform to a vertical mass-spring-damper system. The response is measured for different wire lengths, whereby detecting the resonance shift in the frequency spectrum it is possible to identify the fundamental of the wire for a particular wire length.

Figure 3.3: Picture of wire measurement.

4
Measurement Results and analysis

In this chapter, the main results of the measurements are presented and analysed.

4.1 Creep groan

All measurements developed sustained creep groan upon operation with a range of stick-slip periodicity and amplitudes, depending on the operation parameters (i.e. brake pressure and ramp speed).

The results produced from 4 mm/s and 8 bar are chosen as the central sample of this thesis. This choice is not motivated by any particular quality, given that any or all of the measurements containing creep groan could be used for validation.

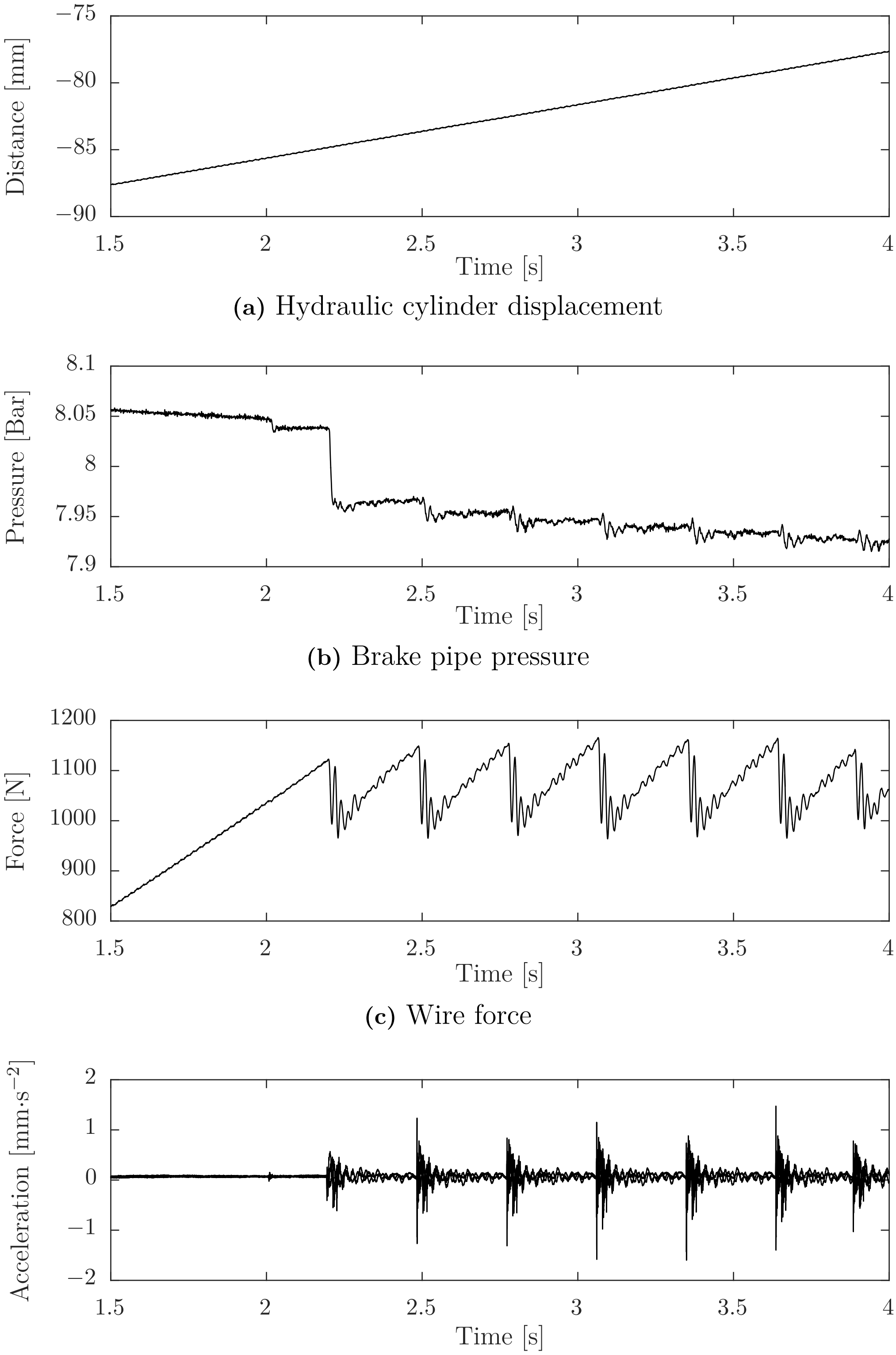

(a) Hydraulic cylinder displacement

(b) Brake pipe pressure

(c) Wire force

(d) Accelerations (all)

Figure 4.1: Data signals measured during creep groan event.

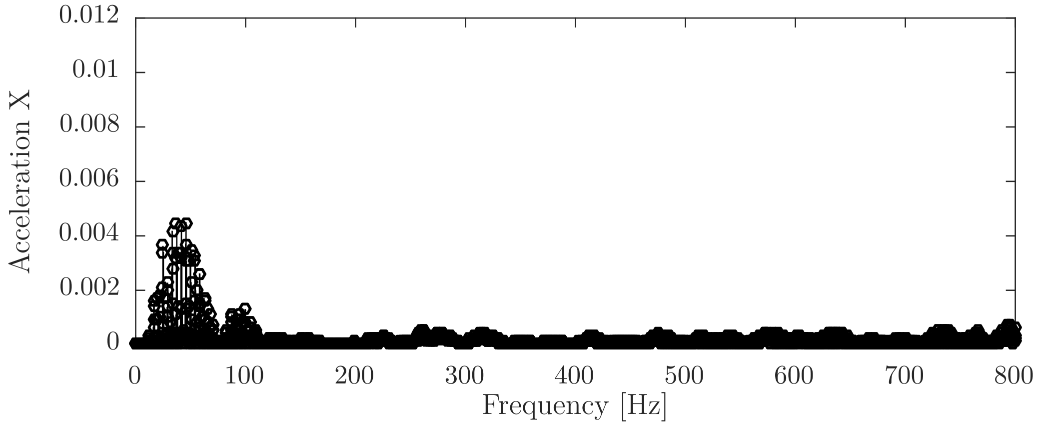

(a) a_1: x

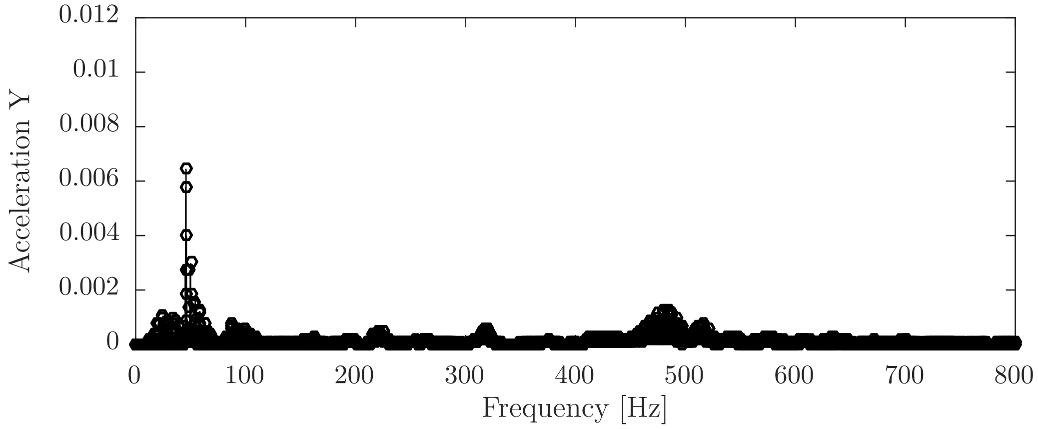

(b) a_1: y

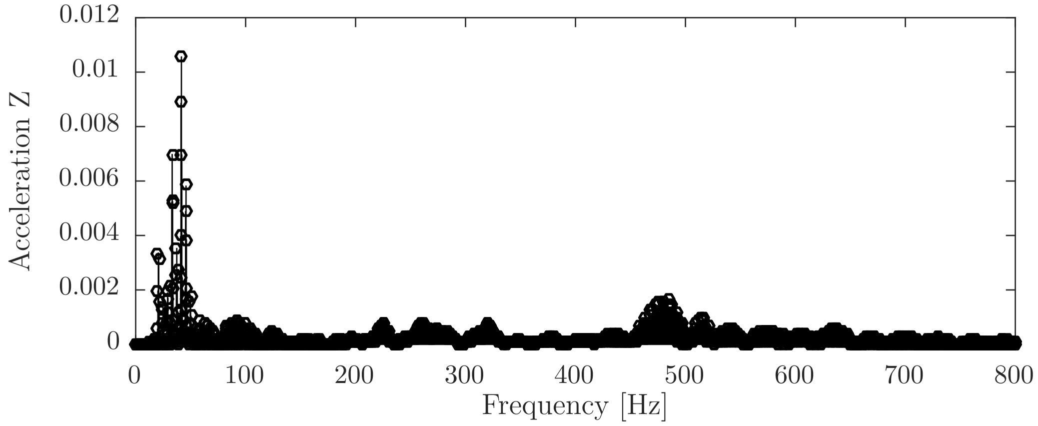

(c) a_1: z

Figure 4.2: Acceleration spectra during creep groan event.

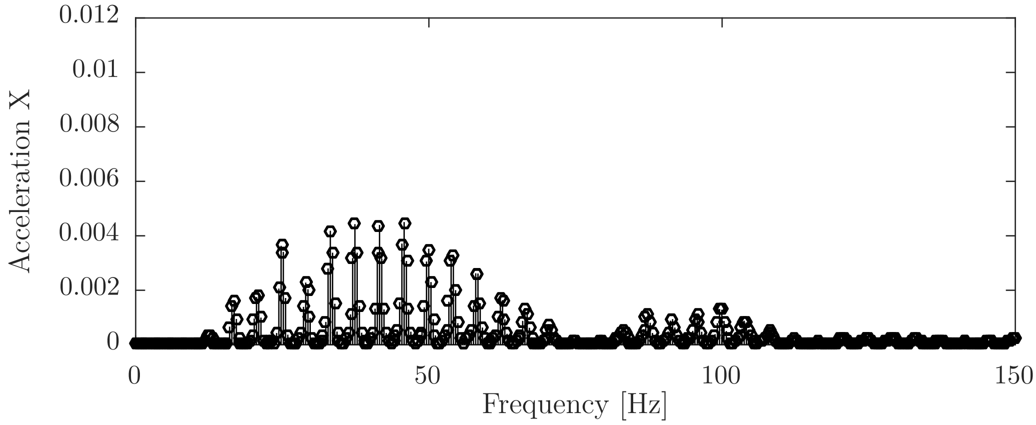

(a) a_1: x

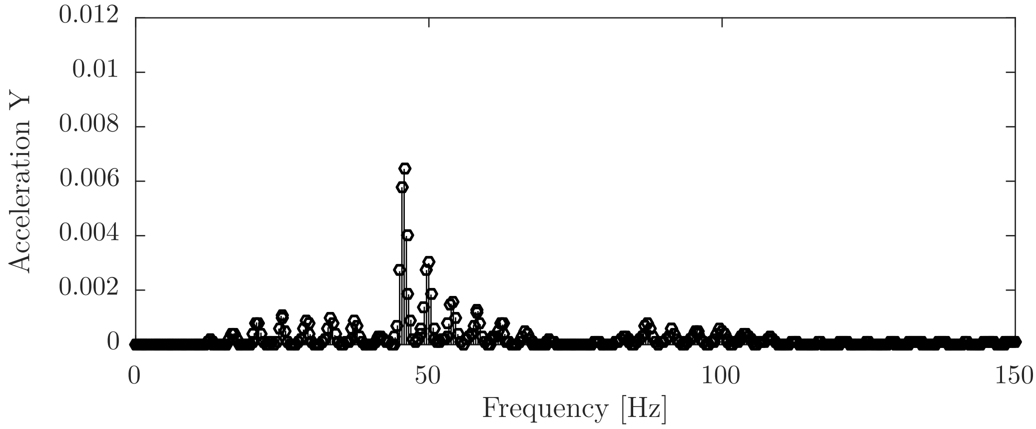

(b) a_1: y

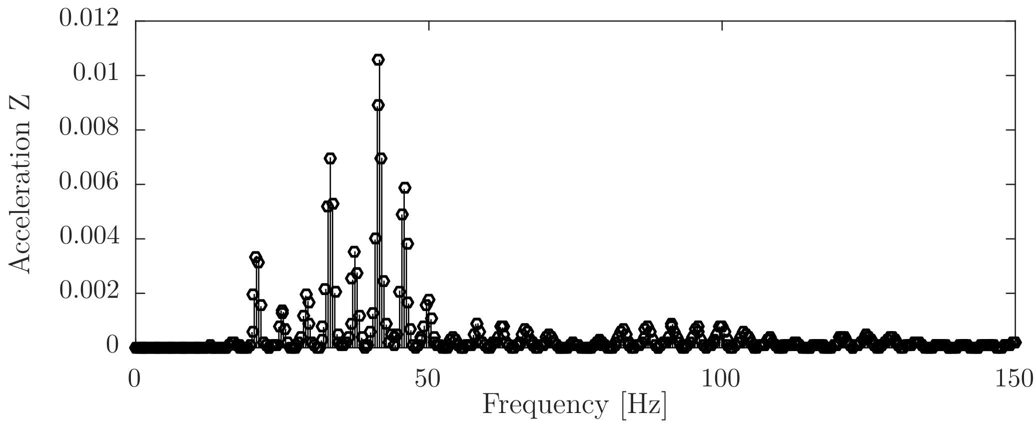

(c) a_1: z

Figure 4.3: Acceleration spectra during creep groan event (zoomed).

4.2 Wire

In the frequency domain, system displacement amplitude for a spring-mass-damper system is calculated from[12]

$$\xi_{\mathrm{visc}}(\omega) = \frac{F_{\mathrm{e}}(\omega)}{-m\omega^2 + j\omega\gamma + k} \tag{4.1}$$

where F_e designates excitation force, m is the mass, γ is the viscous damping, k is the spring constant and ω is the angular velocity. The system eigenfrequencies are solutions for Equation (4.1) that tend toward infinity for an arbitrary force *i.e.,* where the denominator tend toward zero. The solution to $-\omega^2 m + j\omega\gamma + k = 0$ is found by employing the PQ-formula

$$\omega_0 = j\frac{\gamma}{2m} \pm \sqrt{\frac{k}{m} - \frac{\gamma^2}{4m^2}}. \tag{4.2}$$

The viscous damping model has a complex impact on resonance frequencies, however, by considering $k/m \gg \gamma^2/(4m^2)$ and ignoring the imaginary, equation (4.2) can be reduced to $\omega_0 = \sqrt{k/m}$.

From Equation (4.2), the stiffness for one particular wire length can be found if the natural frequency and mass is known. While the mass was simply weighted to 10 kg, the resonance is found from repeating the measurement with a different wire length, and identifying shifted frequencies. The two measurements are plotted in Figure 4.4, where the resonance increases in frequency between takes A and B from $f_{0,\mathrm{A}} = 26.5 \rightarrow f_{0,\mathrm{B}} = 39.4$ Hz and consequentially, k_{A} and k_{B} can be found.

In order to calculate the stiffness for a cable of any length, L_{x}, first consider that the axial stiffness of the cable is defined as the ratio

$$k_{\mathrm{n}} \equiv \frac{AE}{L_{\mathrm{n}}}, \tag{4.3}$$

where A is the cross-sectional area, E is the elastic modulus and L is the element length. Granted that the wire only changes in length (the numerator in equation (4.3) remain unchanged), a general expression for spring stiffness can be derived

$$k_{\mathrm{B}}L_{\mathrm{B}} = AE = k_{\mathrm{x}}L_{\mathrm{x}} \Rightarrow k_{\mathrm{x}} = k_{\mathrm{B}}\frac{L_{\mathrm{B}}}{L_{\mathrm{x}}} = \omega_{0,\mathrm{B}}^2 m\frac{L_{\mathrm{B}}}{L_{\mathrm{x}}}. \tag{4.4}$$

With $\omega_{0,\mathrm{B}} = \{f_{0,\mathrm{B}} = 39.4\} = 247.56$ rad·s^{-1}, $m = 10$ kg, $L_{\mathrm{B}} = 0.33$ m yields the scaling equation

$$k_x = (2.02 \times 10^5)L_x^{-1}. \tag{4.5}$$

In physical terms, damping is the irreversible process of energy dissipated from oscillations by frictional or other resistive forces. It has the effect of reducing oscillation amplitude over time/rotation. As there is no direct mean for finding the viscous damping, it will be derived from hysteretic damping theory. Note that hysteretic damping models are noncausal (depends on future inputs) and cannot be used for simulations as it forbids integration over time. In the case of hysteretic damping, system displacement amplitude in the frequency domain is

$$\xi_{\mathrm{hyst}}(\omega) = \frac{F_{\mathrm{e}}(\omega)}{-m\omega^2 + k(j\eta + 1)}, \tag{4.6}$$

where η is the hysteretic damping ratio, that is, the share of kinetic energy dissipated in one complete rotation.

By the assumption that the damping only affect wire resonance frequencies by negligible amounts at low frequencies, equations (4.1) and (4.6) are combined $\xi_{\mathrm{visc}}(\omega_0) = \xi_{\mathrm{hyst}}(\omega_0)$, so $\eta k = \omega_0 \gamma \Rightarrow \gamma = \eta \sqrt{k^2 \big/ \frac{k}{m}}$. Now arriving at

$$\gamma = \eta_0 \sqrt{mk}, \tag{4.7}$$

where η_0 is the hysteretic damping ratio at the fundamental, which can be found from the measurement using the half-power bandwidth method:

$$\eta_0 = \frac{\Delta f}{f_0} = \frac{f_2 - f_1}{f_0}, \tag{4.8}$$

where f_0 is the fundamental frequency and Δf is the half-power bandwidth. With values $f_{1,\mathrm{B}} = 38.5$, $f_{2,\mathrm{B}} = 40.7$, $f_{0,\mathrm{B}} = 39.4$ equation (4.7) yields

$$\gamma_x = 25.08 L_x^{-0.5} \tag{4.9}$$

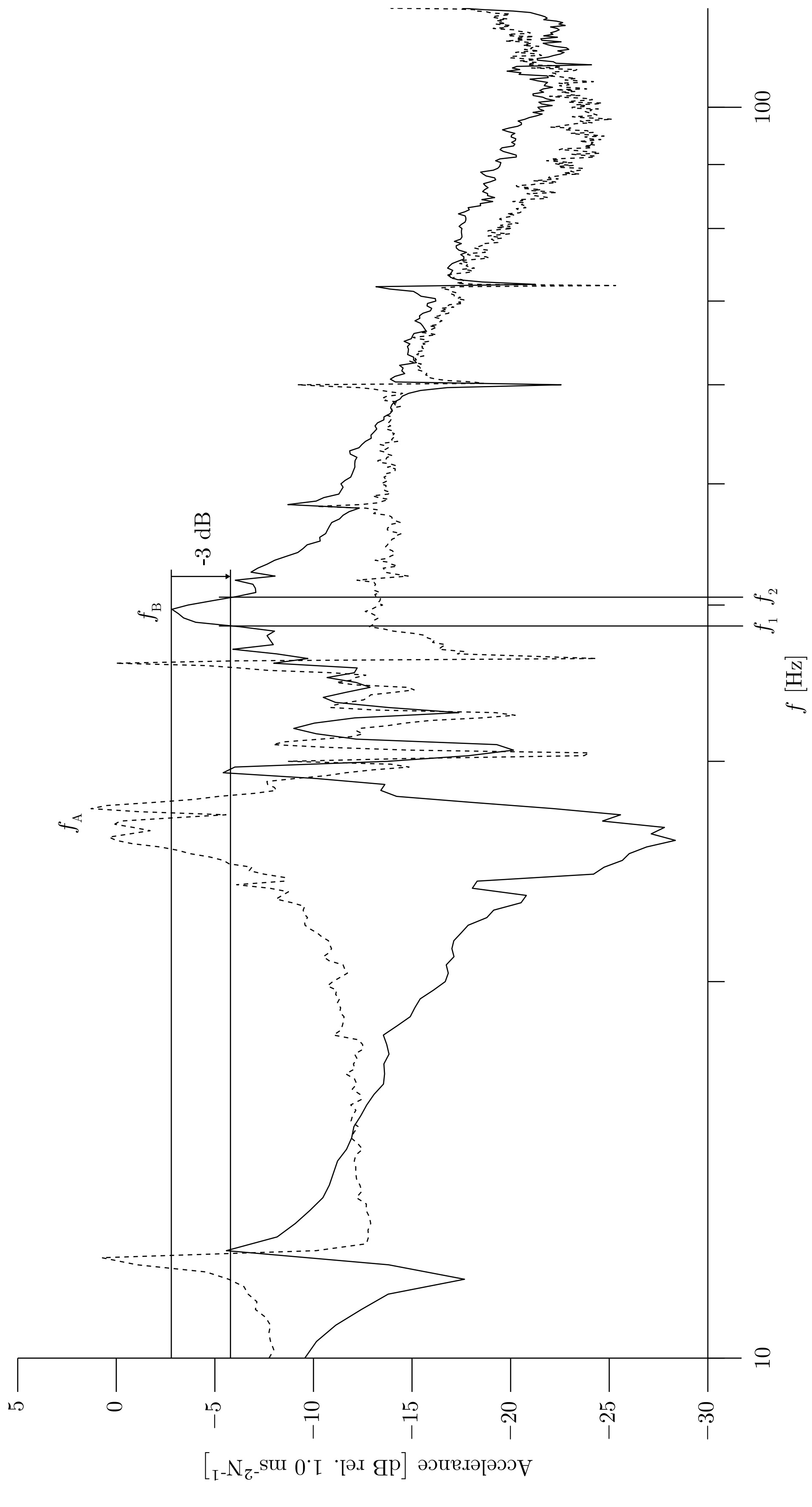

Figure 4.4: System response for L_{A} (- - -) and L_{B}(=0.33 m) (—), each 1st mode identified by f_{A} and f_{B}. Demonstration of determining wire loss factor parameters at f_{B} by half-power bandwidth method.

4.3 Rig analysis

4.3.1 Operating deflection shape

Operating deflection shape (ODS), is a method used for determining vibration patterns of structures under unknown load or operating conditions. An ODS analysis provides a means of identifying mode shapes and their eigenfrequencies, which is necessary information when later verifying the computer model. It is achievable as the acceleration measurements are performed at different positions and directions on the brake rig. However, as the modal number increases, so does its complexity and consequentially more measurement points are required. In the measurements, the number of accelerometers used only allows for accurately representing the first few modes, however, as creep groan is principally a low frequency phenomena the 9 accelerometers are expected to suffice.

A spectral ODS analyzer was programmed in MATLAB that utilize the data and metadata from the measurements to animate the vibration of the structure at chosen frequencies (see Appendix C for code).

With knowledge of the mechanics of stick-slip and by studying Figure 3.2 and/or , it is possible to make assumptions on what modes will receive the largest vibrations upon operation. It is easy to see how during stick criterion, as the hydraulic cylinder contracts, it will displace and create a translational tension for the whole structure but also a rotational tension for the knuckle. Once the stick criterion fails and slip occurs, these tensions will release and excite any such translational and rotational modes in particular. The purpose of the ODS is to identify these 'primary modes', to later use their eigenfrequency as benchmarks for the computer model.

Table 4.1: Primary modes revealed from ODS.

	Mode shape	Hz
ODS mode A	Translational	25 Hz
ODS mode B	Rotational	41 Hz

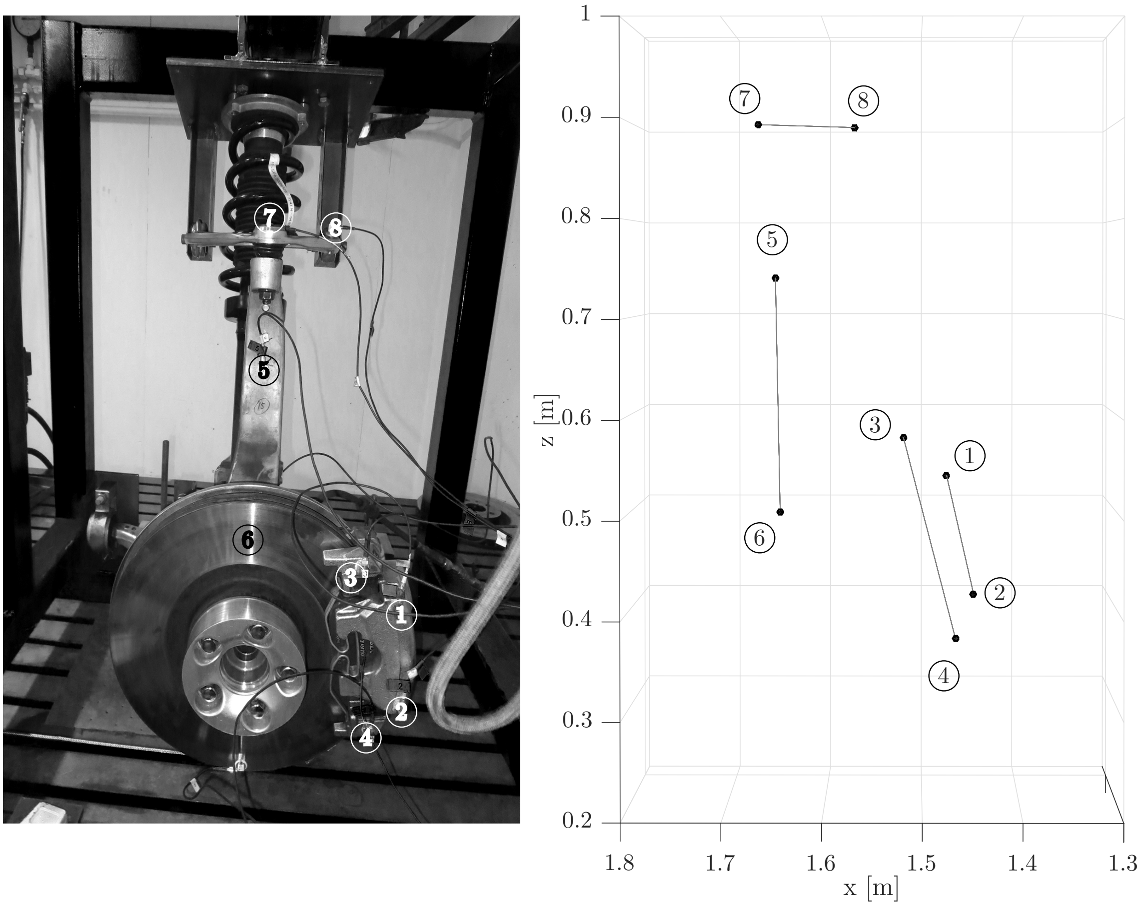

Figure 4.5: Side by side display of Brake rig and ODS with accelerometer numbering

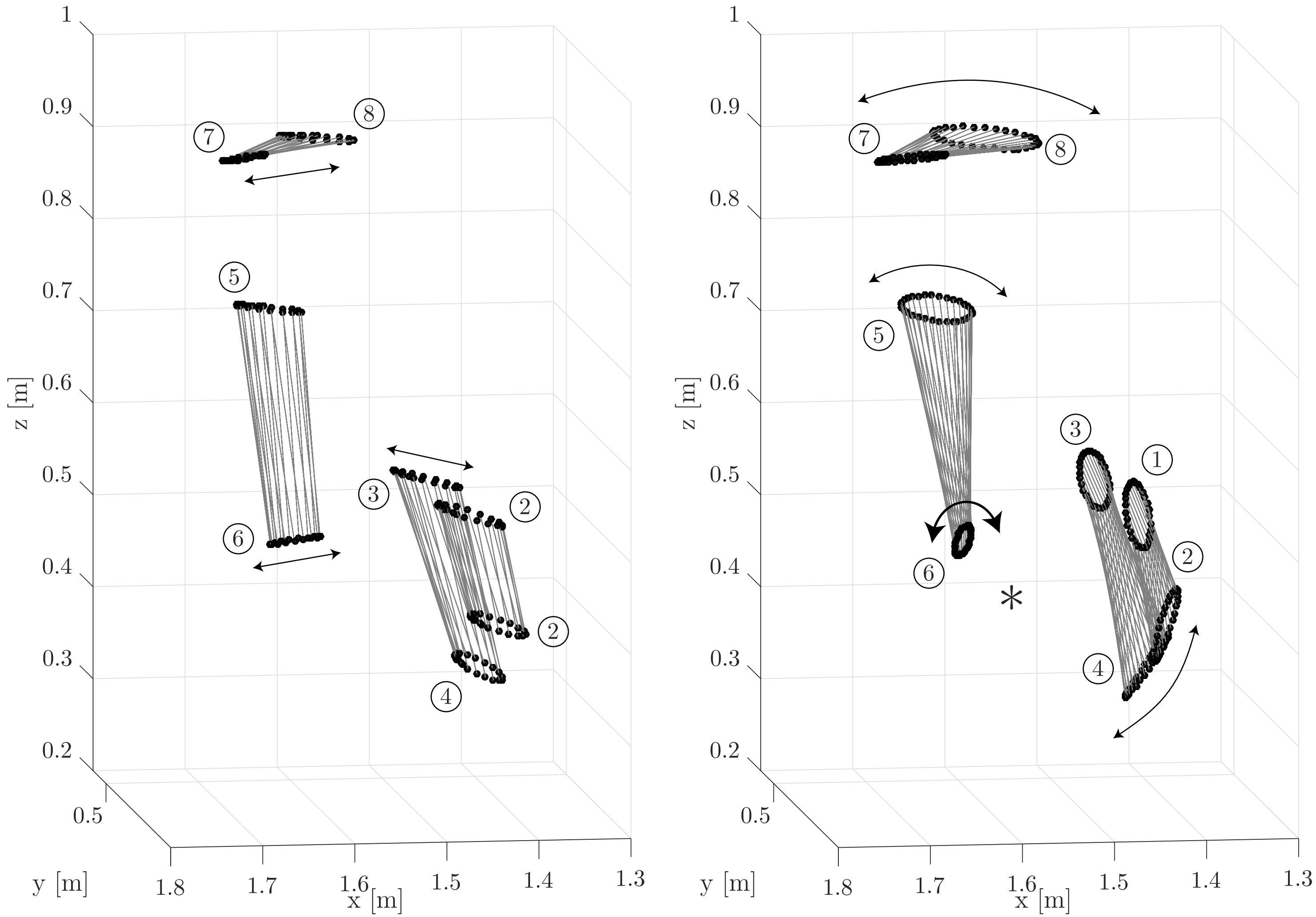

(a) 25 Hz, ODS mode A

(b) 41 Hz, ODS mode B

Figure 4.6: Traced ODS animation of primary modes. Black dots symbolize accelerometers, grey lines symbolize connectivity and asterisk (∗) symbolize pivot point.

4.3.2 Static coefficient of friction

The geometry of the disc and brake is presented in Figure 4.7

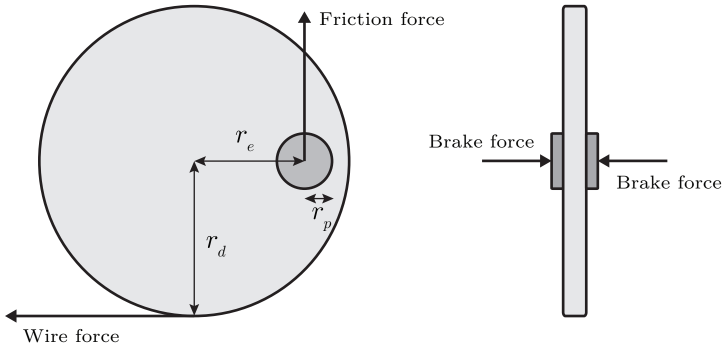

Figure 4.7: Illustration and descriptions of disc/brake geometries.

Where the disc radius is $r_d = 0.18$ m, the brake effective radius is $r_e = 0.137$ m, piston pressure is $p = 7.8 \times 10^5$ Pa and piston radius is $r_p = 30 \times 10^{-3}$ and the maximum force as seen in Figure 4.1 is $F = 1100$ N. From torque equilibrium we can calculate the static friction coefficient

$$\mu_\mathrm{k} = \frac{1}{2} \frac{F r_d}{(r_p^2 \pi p) r_e} = 0.34 \tag{4.10}$$

5
Multi-body model

Using ADAMS, a multibody model is created that aims to replicate the brake system rig as set-up in the experimental measurements in both design and function.

5.1 Geometry

The full geometry of the model is comprised of parts, assembled similarly as it was in the experiment. The geometry (or bodies) imported into ADAMS falls into one of two categories, that is, 'rigid bodies' or 'flexible bodies'.

Table 5.1: Components included in ADMAS model.

Component	Bodytype
Ground	Ground
Caliper	Rigid Lumped Mass
Outer back plate	Rigid Lumped Mass
Inner back plate	Rigid Lumped Mass
Outer pad	Rigid Lumped Mass
Inner pad	Rigid Lumped Mass
Disc	Rigid Lumped Mass
Console A	Flexible body
Console B	Flexible body
Console C	Flexible body
Upper control-arm	Flexible body
Tierod	Flexible body
Knuckle	Flexible body
Lower control-arm	Flexible body
Ball-joint bracket	Flexible body
Fork	Flexible body
Hydraulic piston	Rigid Lumped Mass
Ghost connector 1	Rigid Lumped Mass
Ghost connector 2	Rigid Lumped Mass

5.1.1 Rigid bodies

In physics, a rigid body is an idealization defined as a body of which the distance between any two points within the body remain constant; such as they cannot deform. Rigid bodies hold mass and inertia properties and can only move relative to other parts. In brief, rigid bodies are warranted by reducing the number of calculations and should be used for parts that are expected to behave rigidly and/or not strongly affect modes that are associated with creep groan.

The rigid bodies are imported from CAD geometries into ADAMS using file format Initial Graphics Exchange Specification (IGES). IGES is a surface format and does not contain volume information: upon import, ADAMS converts the shell to a solid feature after which, each parts respective density is set and consequentially its mass and inertia is applied. By the manner of comparing the real mass to the calculated mass in ADAMS, each part is proof-checked to be correctly imported.

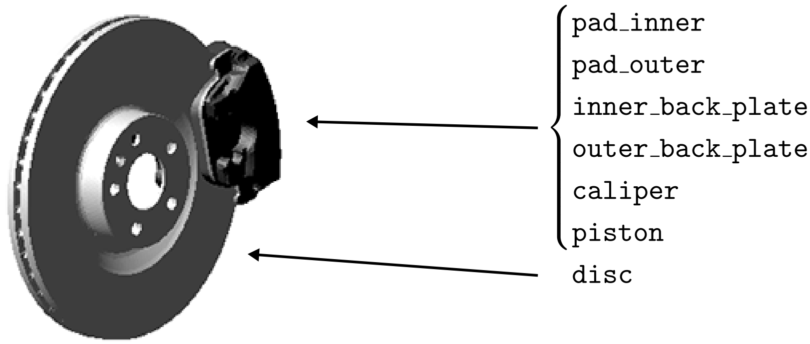

Figure 5.1: Rigid bodies of model.

Modelling the parts in Figure 5.1 as rigid pertain to their position and compactness/heftiness relative to other parts in the model. The impact of primary mode shapes and frequencies by account of these rigid bodies are expected to be negligible.

5.1.2 Flexible bodies

As shown from the acceleration spectra and ODS analysis, creep groan excite certain structural modes. In order to capture the same behaviour in the computer model, key parts are modelled as flexible bodies. Flexible bodies are described by Modal Neutral File (MNF) contains a range of data blocks that describes the physics, *e.g.*, geometry, mass and mode shapes for each individual component.

It should be acknowledged that this thesis project did not involve creating these features, as they had been previously generated at VCC.

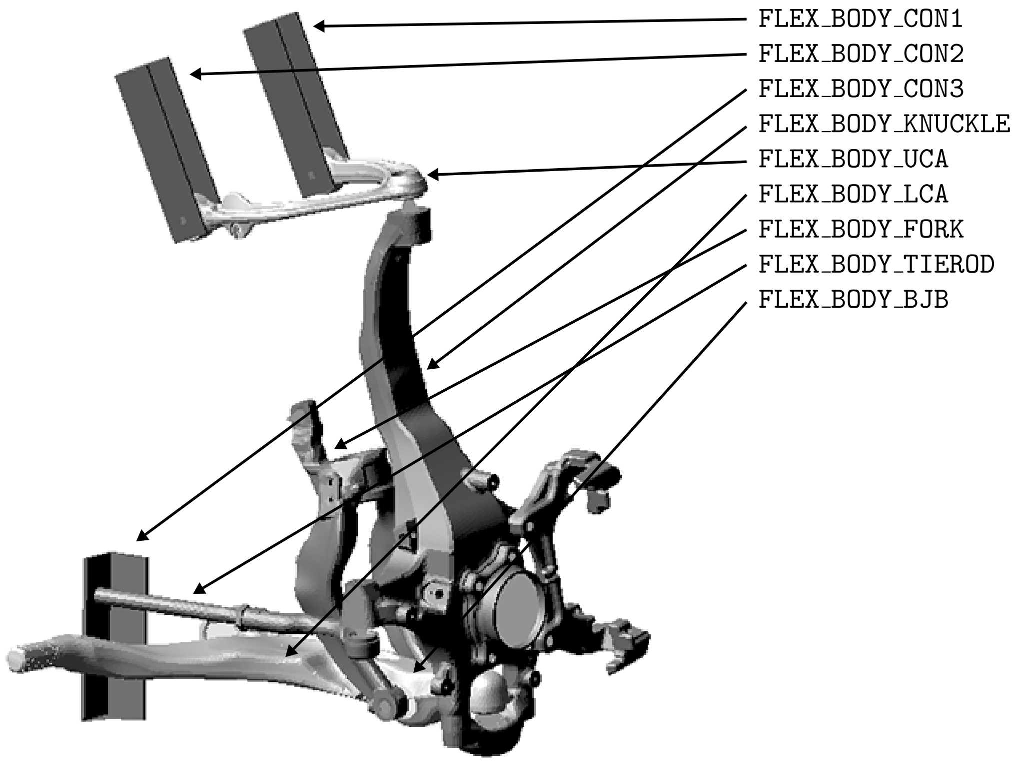

Figure 5.2: Flexible bodies of model.

5.2 Topology

By default, each imported or created body into ADAMS can move freely within six degrees of freedom and so the bodies are free to change spatially in any which direction or rotation: up–down, forward–back, left–right, pitch, yaw, roll. In other words, once all parts are imported and assembled into ADAMS the model must also be constrained to mechanically represent the brake system. This is achieved by constraining the model with joint connectors, flexible connectors, forces and motions:

- Joint connectors describes how two parts may move relative another.
- Flexible connectors governs the forces between two parts as they move relative another.
- Forces is a vector that acts on an object
- Motions impose a change in position of an object

Table 5.2: Topology of creep groan model

Constraint name		Part		Part	Constraint type
JOINT_FIX_PO_OBP	connects	pad_outer	with	outer_back_plate	Fixed Joint
JOINT_FIX_PI_IBP	connects	inner_back_plate	with	pad_inner	Fixed Joint
JOINT_TRANS_CALI_PIST	connects	piston	with	caliper	Translational Joint
JOINT_FIX_PIST_IBP	connects	piston	with	inner_back_plate	Fixed Joint
JOINT_FIX_CALI_OBP	connects	outer_back_plate	with	caliper	Fixed Joint
SFORCE_CHAMBER	connects	piston	with	caliper	Single Component Force
JOINT_9	connects	FLEX_BODY_CON3	with	ground	Fixed Joint
JOINT_10	connects	FLEX_BODY_CON3	with	FLEX_BODY_TIEROD	Fixed Joint
JOINT_11	connects	FLEX_BODY_TIEROD	with	FLEX_BODY_KNUCKLE	Spherical Joint
JOINT_12	connects	FLEX_BODY_KNUCKLE	with	FLEX_BODY_UCA	Spherical Joint
JOINT_13	connects	ground	with	FLEX_BODY_CON1	Fixed Joint
JOINT_14	connects	ground	with	FLEX_BODY_CON2	Fixed Joint
JOINT_17	connects	FLEX_BODY_BJB	with	FLEX_BODY_LCA	Spherical Joint
JOINT_23	connects	caliper	with	FLEX_BODY_KNUCKLE	Cylindrical Joint
JOINT_24	connects	caliper	with	FLEX_BODY_KNUCKLE	Cylindrical Joint
JOINT_25	connects	PART_10	with	FLEX_BODY_BJB	Fixed Joint
JOINT_26	connects	FLEX_BODY_KNUCKLE	with	PART_10	Fixed Joint
JOINT_27	connects	FLEX_BODY_BJB	with	PART_11	Fixed Joint
JOINT_28	connects	FLEX_BODY_KNUCKLE	with	PART_11	Fixed Joint
JOINT_29	connects	FLEX_BODY_KNUCKLE	with	disc	Revolute Joint
JOINT_30	connects	ground	with	PART_12	Translational Joint
BUSHING_1	connects	FLEX_BODY_CON2	with	FLEX_BODY_UCA	Bushing
BUSHING_2	connects	FLEX_BODY_UCA	with	FLEX_BODY_CON1	Bushing
BUSHING_3	connects	FLEX_BODY_LCA	with	ground	Bushing
BUSHING_4	connects	FLEX_BODY_LCA	with	ground	Bushing
BUSHING_5	connects	FLEX_BODY_FORK	with	FLEX_BODY_LCA	Bushing
CONTACT_FRIC_INNER	connects	pad_inner	with	disc	Contact
CONTACT_FRIC_OUTER	connects	pad_outer	with	disc	Contact
SPRING_2.sforce	connects	disc	with	PART_12	Single Component Force
SPRING_1.sforce	connects	FLEX_BODY_FORK	with	ground	Single Component Force

5.2.1 Joint connectors

Joints restrict relative movement between two parts and represent idealized physical connections. Once a joint is added between two parts, particular DOF's associated with said joint are removed between the parts, forcing them to behave in the prescribed manner regardless of any imposed force or motion. As a consequence, joints tend to 'overvalue' the structural stiffness to some degree.

Five types of joints were used in the model, they include: fixed, translational, spherical, revolute and fixed. These can be understood by the type and number of freedoms they remove, which is documented in Table 5.3.

Table 5.3: Number of DOF's removed for joints.

		Rotational			
		0	1	2	3
Translational	0				
	1				
	2			Cylindrical	Translational
	3	Spherical		Revolute	Fixed[1]

Cataloging the behaviour of every joint constraint used in the model would be an overambitious and redundant effort. The reader is referred to cross-examining tables 5.2 and 5.3.

5.2.2 Applied forces

Forces in ADAMS, much like in reality, can be defined as an interaction that brings dynamic to a system. Forces can both act and react between parts and can be utilized in many which ways depending on how they are programmed. In the model, forces were used to describe the wire, suspension spring, bushings and braking force.

The wire is modelled as a damped spring, with properties following equations (4.5) and (4.9) for a wire of length 0.57 m. The suspension spring was also modelled as a damped spring, though in this case, values for stiffness and damping is retrieved from the engineering department and set to 63.8 N/mm and 11.2 Ns/mm respectively. Each bushing is modelled using the pre-defined bushing tool that apply springs and dampers in all directions and rotations. Data of the nominal bushing parameters was retrieved from the engineering department and is presented in Table 5.4. Braking force is modelled as a constant force and is calculated from the pistons pressure and area. Given a pressure of 8 bar and a piston radius of 30 mm, the braking force is set to 2200 N.

[1]Parts fixed to the ground are completely locked in its inertial space.

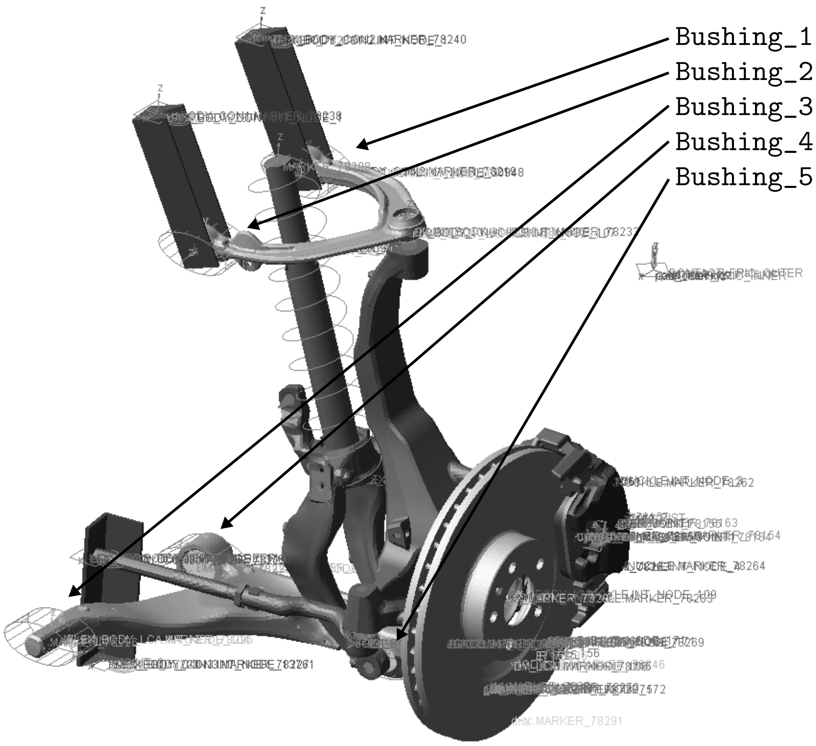

Figure 5.3: Bushing placements.

Table 5.4: Nominal bushing parameters

	Translational properties		Rotational properties	
	Stiffness [N/mm] (x,y,z)	Damping [Ns/mm] (x,y,z)	Stiffness [N/rad] (x,y,z)	Damping [Ns/rad] (x,y,z)
`Bushing_1`	(5000,5000,900)	(0.232,0.232,0.041)	(3.437E+5,3.437E+5,1.145E+5)	(0.001,0.001,0.001)
`Bushing_2`	(5000,5000,900)	(0.232,0.232,0.041)	(3.437E+5,3.437E+5,1.145E+5)	(0.001,0.001,0.001)
`Bushing_3`	(45000,45000,1500)	(2.088,2.088,0.069)	(2.291E+6,2.291E+6,2.864E+5)	(0.001,0.001,0.001)
`Bushing_4`	(4400,1080,500)	(0.204,0.050,0.023)	(2.291E+5,8.594E+5,2.291E+5)	(0.001,0.001,0.001)
`Bushing_5`	(40000,40000,3000)	(1.856,1.856,0.139)	(3.437E+6,3.437E+6,3.437E+5)	(0.001,0.001,0.001)

5.2.3 Contact

Bodies in ADAMS do not collision in simulations by default. One body may intersect another without interacting as if they were made out of nothing. For ADAMS to recognise a collision, such as the pad–disc interface(s), a contact constraint can be applied between the parts.

ADAMS has two in-built algorithms for modelling contact normal forces, called impact and restitution, of which the former was chosen. When modelling a stick-slip contact interface the impact algorithm can be regarded favorable for its robustness in numerical integration, as in comparison to restitution, it computes faster and is more smooth[2]. Also, restitution is not particularly well-suited for modelling the sustained types of contacts mostly occurring in creep groan[2].

The impact algorithm functions by introducing a damped spring between the bodies once they intersect, acting to undo and impede the collision. Specifically, the damped spring is located between the closest points of the intersection's center of mass to each body's surface and its force is governed by

$$F_{\text{n,impact}} = \begin{cases} 0 & \text{if } x_1 < x \\ k(x_1 - x)^e - c_{\max}\dot{x} \cdot \texttt{step}(x, x_1 - d, 1, x_1, 0) & \text{if } x_1 \geq x \end{cases}. \tag{5.1}$$

In equation (5.1), x and x_1 are algorithmic values pertaining to the relations of the bodies. The other parameters are user defined and explained in the paragraph below along with how they were determined for the simulation(s).

Stiffness, k, describes the force required for each unit of penetration depth and depends on both the materials elastic properties and their geometry. Consequentially it can be troublesome determining an exact value of k. In this thesis, k was approximated by running multiple equilibrium simulations with different values of k to see what value grants realistic penetration depths. From the simulations, the stiffness was decided and set to 1×10^5 N/mm. The force exponent, e, represent a non-linearity option to the spring force where the force can be set to exponentially increase by intersection depth. This is related to the materials resistance to changing shape when a compressive force is applied. For hard metals such as the disc, ADAMS recommends a value of $e \simeq 2.2$, however as the pad is expected to be softer, the force exponent was lowered to $e = 2.0$. Maximum damping coefficient, $c_{\max}$, is the upper limit of the step function that rule how much damping is used. It generally takes a value of $0.01 \times k$ or lower, the value of $c_{\max}$ changed between simulations[3]. Penetration depth, d, is the other limit to the step function that rule at what depth maximum damping is applied. It should be lower than equilibrium penetration depth, and so it is set to 0.1 mm.

[2]Restitution is preferably applied to 'transient contacts' such as impulses.

[3]For reasons and implications unknown: It was noticed that the maximum damping parameter influenced convergence significantly for some bushing values and regularization parameters, and so it was changed (within the $c_{\max} < 0.01 \times k$ bound) in some instances to avoid overwhelming run times.

In addition to a mandatory normal force, contact constraints also feature a friction option. Similarly to the models presented in section 2.2, ADAMS also uses a differentiable regularized friction curve, albeit modelled differently using smooth step functions as opposed to a single expression. The friction coefficient in ADAMS is written on the form

$$\mu(v) = \begin{cases} -\texttt{sgn}(v) \cdot \mu_{\mathrm{d}} & \text{for } |v| > v_{\mathrm{d}} \\ -\texttt{step}(|v|, v_{\mathrm{d}}, \mu_{\mathrm{d}}, v_{\mathrm{s}}, \mu_{\mathrm{s}}) \cdot \texttt{sgn}(v) & \text{for } v_{\mathrm{s}} \leq |v| \leq v_{\mathrm{d}} \\ \ \texttt{step}(v, -v_{\mathrm{s}}, \mu_{\mathrm{s}}, v_{\mathrm{s}}, -\mu_{\mathrm{s}}) & \text{for } -v_{\mathrm{s}} < v < v_{\mathrm{d}} \end{cases} \tag{5.2}$$

such as

- $\mu(-v_{\mathrm{s}}) = \mu_{\mathrm{s}}$
- $\mu(v_{\mathrm{s}}) = -\mu_{\mathrm{s}}$
- $\mu(0) = 0$
- $\mu(-v_{\mathrm{d}}) = \mu_{\mathrm{d}}$
- $\mu(v_{\mathrm{d}}) = -\mu_{\mathrm{d}}$

where all the parameters are set by the user to create a contact interface that suits the application.

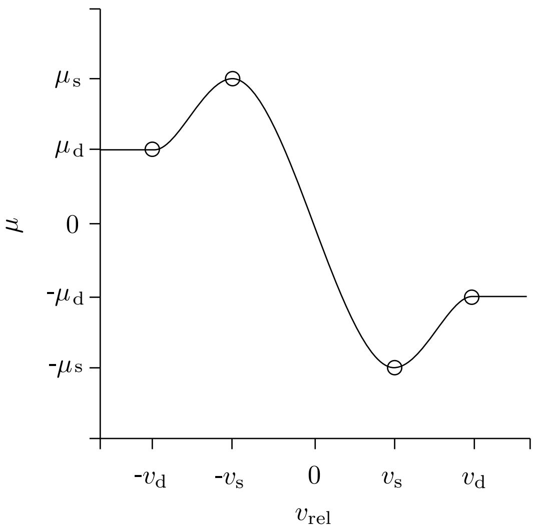

Figure 5.4: Coefficient of friction vs relative velocity in ADAMS

The static friction coefficient (μ_{s}) is set to 0.34 as calculated from the measurement and the dynamic friction coefficient (μ_{d}) is approximated to 0.26. Stiction friction slip velocity (v_{s}) is the relative velocity at which full static friction is applied and dynamic friction transition velocity (v_{d}) is the relative velocity at which friction has fully transitioned into dynamic friction. In general, the closer v_{s} and v_{d} are to zero, the more accurate the physical description becomes, however the ODE stiffness will also increase meaning there has to be compromise between accuracy and numeric instability (i.e. if v_d assumes a very large value in relation to substrate speed the dynamic friction will have no impact on dynamics, and on the other hand if it assumes a very small value, it would increase numerical instability). Ultimately, after running multiple simulations, stiction and dynamic transitions velocities are set to $v_\mathrm{s} = 6.0 \times 10^{-2}$ mm/s and $v_\mathrm{d} = 1.8$ mm/s, at which point, lowering their values did not bring noticeable change in dynamics.

5.2.4 Driving constraint

In the experiment, the brake system is put into motion by the hydraulic cylinder, contracting the piston and pulling the end of the wire at a constant pace of 4 mm/s. In the ADAMS model this is replicated by connecting spring force to a part that is constrained to a translational joint, for which the remaining DOF is constrained to a constant translational motion.

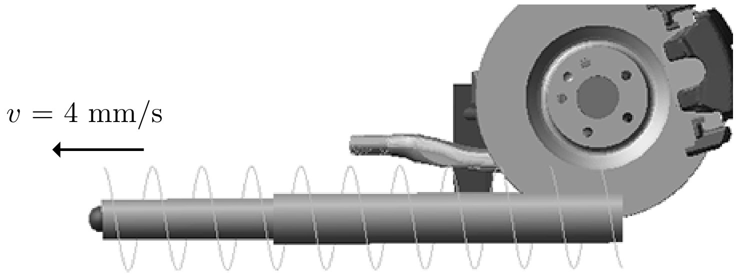

Figure 5.5: Driving constraint.

5.3 Solver settings

As the model contain more than one degrees of freedom and as forces affect vibrations, the model is solved dynamically, as opposed to kinematically. There are different methods of solving dynamic systems and these methods are referred to as integrators. The integrator in ADAMS has multiple options and lets you format the numerical integration process for accuracy and efficiency relating to particular motions and dynamics.

Taking into consideration the rapid change in friction coefficient at stick-slip transition means the system contain numerically unstable properties, thus a very small stepsize is required for an accurate solution. However, the instability is mostly dormant and it would be inefficient to solve the non-stiff regions with the same small stepsize. Therefore, the system is solved using `GSTIFF`, which adapts integration based on the highest current active frequency[2]. To avoid drift-off errors and for further robustness, `SI2` formulation is used in conjunction with the integrator.

6

Model analysis and validation

The simulation results are tried qualitatively and quantitatively to the experimental data. For the scope of this thesis, the model is deemed qualitatively analogous to the experiment if it captures the same behaviour in terms of stick-slip and primary modes.

Granted the behaviour is validated, a quantitative comparison occurs where the accuracy of system response is evaluated. Model parameters are then calibrated to try and improve model accuracy. This process of simulation, validation and calibration repeats until sufficient model predictions are achieved.

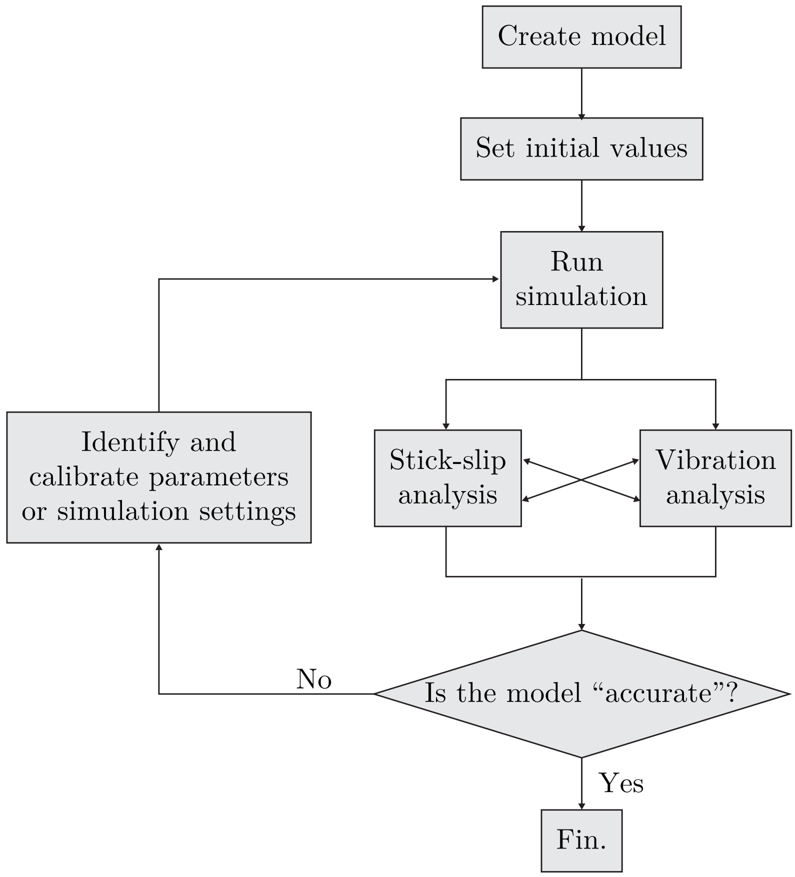

Figure 6.1: Modelling-simulation flowchart.

6.1 Stick-slip analysis

The presence of stick-slip within the simulation can be explicitly shown by plotting the angular (relative wheel hub) velocities of the disc and caliper.

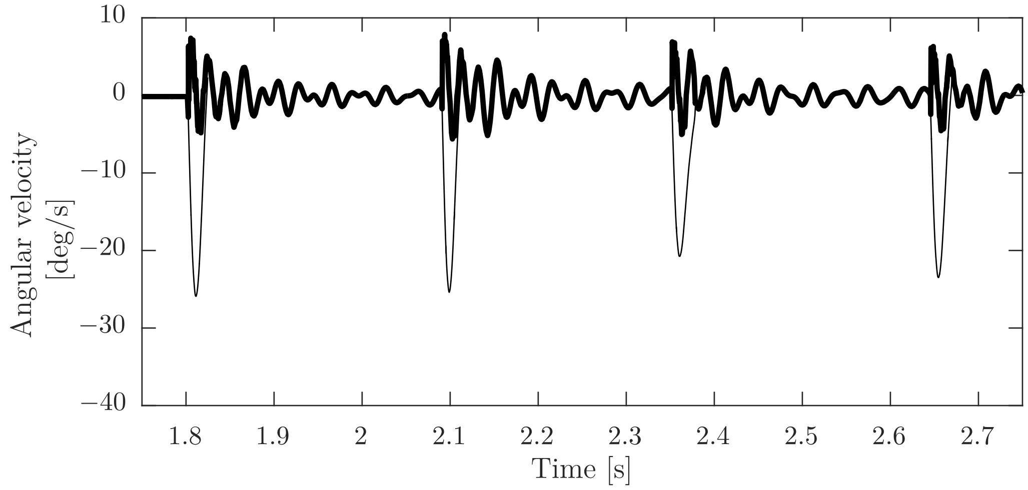

(a) v_{caliper} (——), v_{disc} (——)

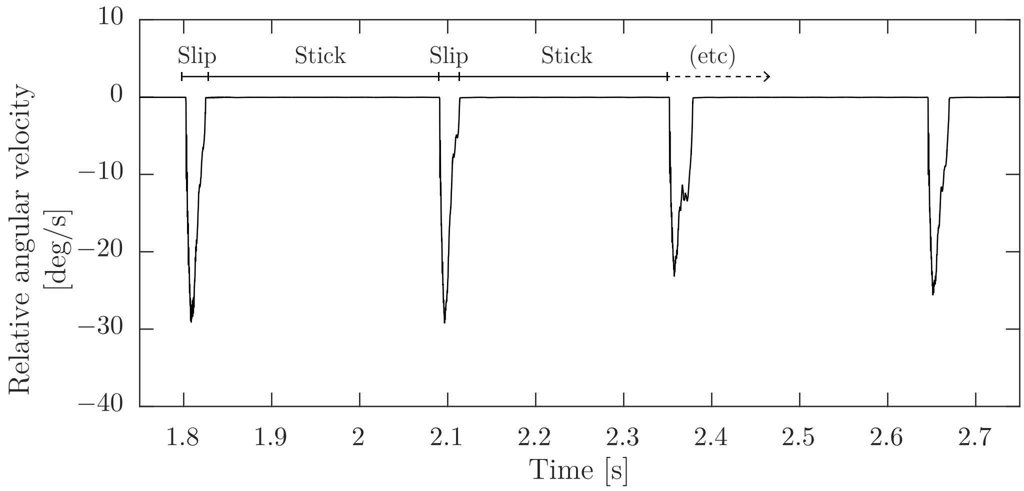

(b) $v_{\text{rel}} = v_{\text{caliper}} - v_{\text{disc}}$

Figure 6.2: Angular velocity time histories of ADAMS simulation during stick-slip oscillation.

With Figure 6.2 (b), the presence of stick-slip within the simulation is clearly demonstrated. During stick, the disc is essentially locked to the rest of the suspension. For slip however, the disc is no longer tangentially constrained with respect to the wheel hub and can rotate semi-independently. As the system will assume two different mechanical configurations during operation it follows that it will contain two different sets of modes. The relation between stick and slip duration approximately follow 1-to-9 in favor of stick.

Upon each slip phase Figure 6.2 (a) shows how potential energy is perpetually translating into kinetic energy and vibration of brake system. A means of evaluating the excitation follows from idealizing the complete rig as a single x-directional spring with force $F_{\mathrm{sp}} = kL$ and potential energy $E_{\mathrm{sp}} = (kL^2)/2$, where k is the spring stiffness and L is the displacement. Potential energy is released into the system upon slip, which occurs once the spring force exceeds static friction force, $F_{\mathrm{s}} = \mu_{\mathrm{s}} F_{\mathrm{n}}$. As the slip phase is relatively short for each stick-slip cycle, displacement can be approximated by $v_{\mathrm{p}}/f_{\mathrm{ss}}$, where v_{p} is the piston speed and f_{ss} is the stick-slip frequency. The potential energy can be rewritten to

$$E_{\mathrm{sp}} = \frac{\mu_{\mathrm{s}} F_{\mathrm{n}} v_{\mathrm{p}}}{2 f_{\mathrm{ss}}}. \tag{6.1}$$

As the piston speed, braking normal force and static friction coefficient are known from the measurement and implemented for the ADAMS model, the implication is that excitation can be assessed in terms of stick-slip frequency

$$f_{\mathrm{ss}}^{\mathrm{sim}} = f_{\mathrm{ss}}^{\mathrm{meas}} \Rightarrow E_{\mathrm{sp}}^{\mathrm{sim}} = E_{\mathrm{sp}}^{\mathrm{meas}}. \tag{6.2}$$

Consequentially, if the stick-slip cycles matches in frequency they can be assumed to produce equal levels of excitation.

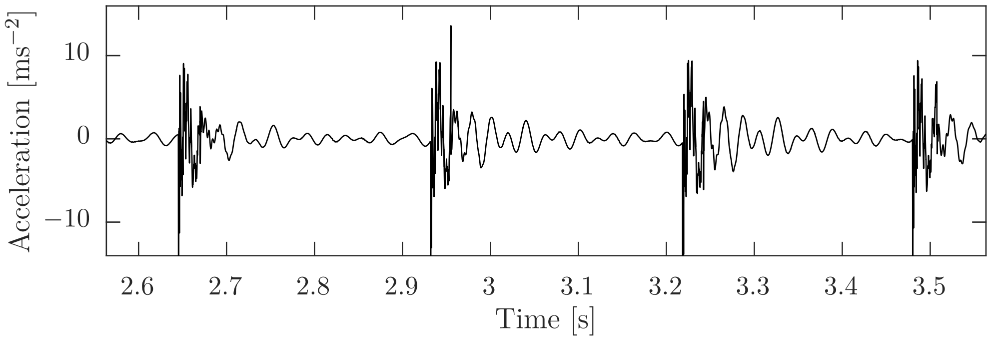

(a) ADAMS simulation

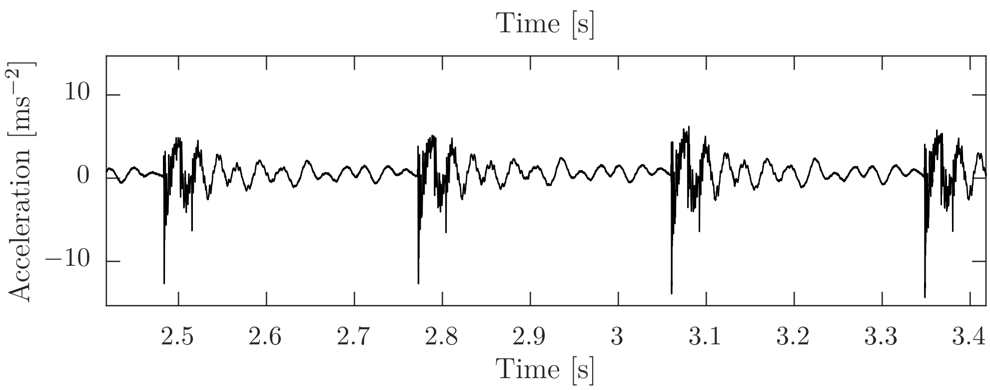

(b) Rig measurement

Figure 6.3: Vertical acceleration time histories of caliper during creep groan.

In terms of cycles, the simulation is found to be accurate toward the measurement with a stick-slip frequency of $f_{\mathrm{ss}}^{\mathrm{sim}} \approx 3.61$ Hz compared to the measurements $f_{\mathrm{ss}}^{\mathrm{meas}} \approx 3.49$ Hz.

Similarly to the experimental results, the model shows some internal variance of stick-slip length. For creep groan, small variance is expected by account of the brake system vibrations which leads to a quickened or delayed slip state as the wire force approaches static friction force limit (consider the wire force fluctuations in Figure 4.1 (c)). The cycle variance of the model is assumed to be primarily limited to this factor, in the physical rig on the other hand there could be outside factors such irregularities of the disc. Unlike the modelled disc, the physical counterpart can for instance have different frictional properties for different angular positions. This non-ergodic disposition inherent to complex stick-slip systems is clearly illustrated with Figure 6.4.

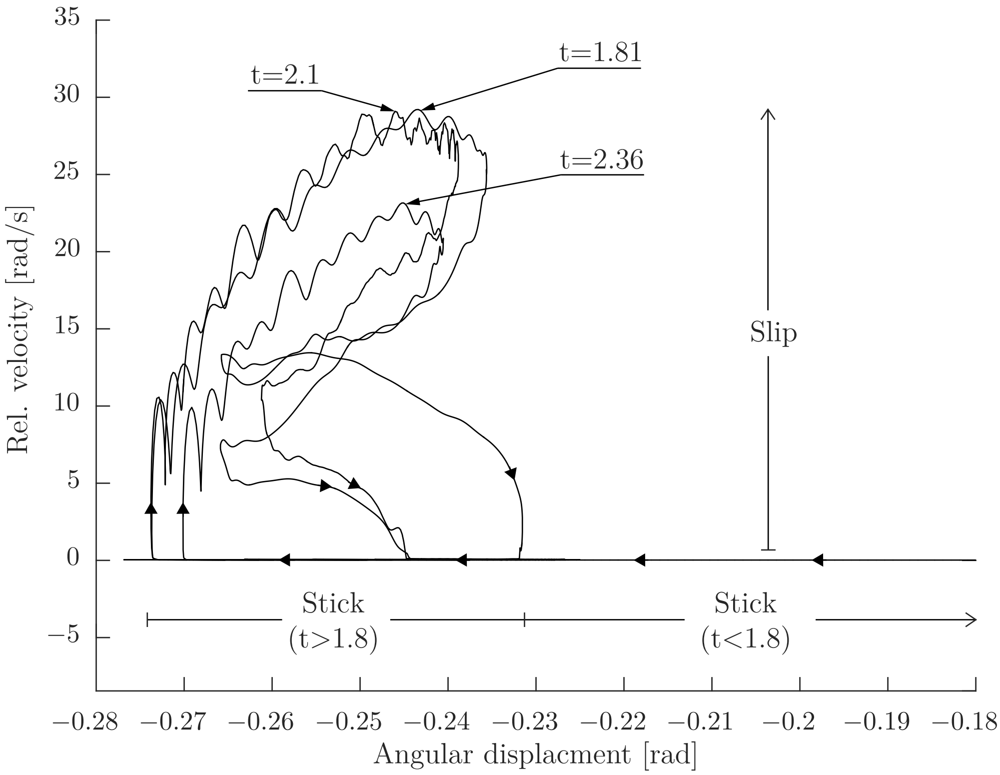

Figure 6.4: Simulation phase plot of caliper displacement and relative velocity with time, direction and state indicators.

The first three stick-slip cycles of the simulation are presented in Figure 6.4 as phase plots where the caliper orbit paths are shown to deviate between different cycles. Approximately, the static friction is overcome for caliper displacements around 15.5° degrees and re-stick occurs for 13.2° $\sim$ 14.0° degrees, indicating that slip phase 'rewinds' the caliper 1.9° degrees on average.

Such metrics would be helpful to compare with the measured data for more in-depth evaluations of overall system behaviour, but also stronger prediction estimates on regularization descriptions and structure properties. However it is not possible as mostly related to AC coupling and coherence: The measured signals are unsound for $f < 10$ Hz and thus stick-slip displacements cannot be accurately integrated.

6.2 Vibration analysis

Figure 6.5 (a) shows the vertical acceleration results in the frequency domain predicted from the numerical simulation, and it can be observed that the accelerations are mostly distributed in the low frequency range similarly as the results from the rig measurement.

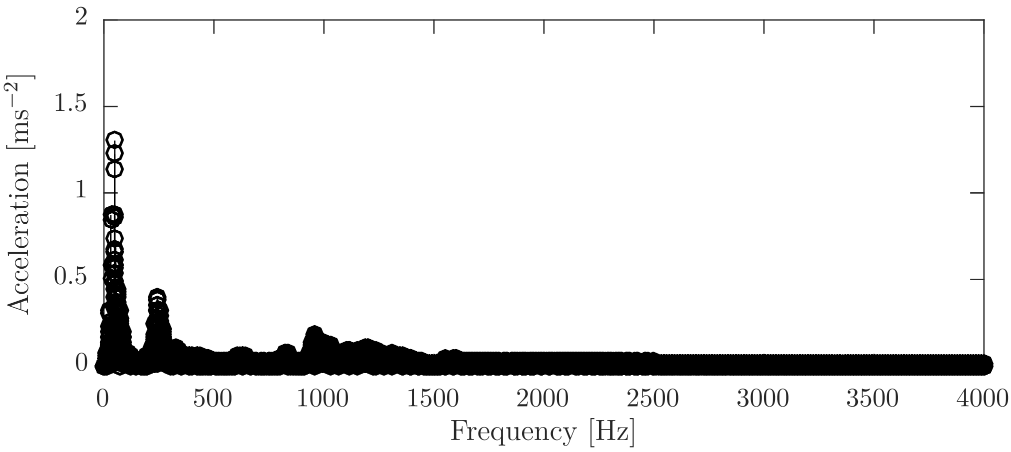

(a) ADAMS simulation

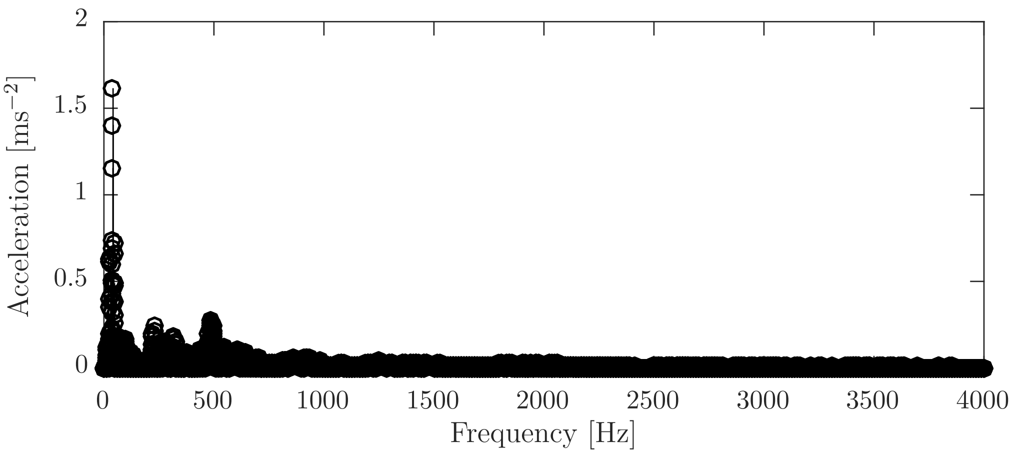

(b) Rig measurement

Figure 6.5: Caliper acceleration (Z) spectra of simulated creep groan event.

For any rigorous validation, the relationship of frequency content and modes must be settled. More specifically it is necessary that it captures equivalent primary modes as found in the ODS analysis, and that they are excited by proportionate amounts.

As opposed to determining mode shapes via ODS analysis, it is approached analytically in ADAMS by linearizing the system at the state of static equilibrium (where all velocities and accelerations are zero and all forces are equilibrated), then solving the system matrices for the nullvector to obtain the eigenvectors and eigenfrequencies.

Note that acceleration spectra is averaged over several stick-slip cycles and thus contains both modal sets. As discovered in the stick-slip analysis: Stick dominates over slip in terms of duration, and so the system is linearized for stick as it is reasonable to assume that modes associated to that configuration most accurately represent the resulting acceleration spectra.

Table 6.1: System eigenvalues at static equilibrium (stick).

Mode number	Undamped natural frequency [Hz]	Damping ratio [c/c_c]	$\mathbb{R}$e		$\mathbb{I}$m
1	1.1194E−003	1.0000E+000	−1.1194E−003	+/−	0.0000E+000
2	1.2641E−001	1.0000E+000	−1.2641E−001	+/−	0.0000E+000
3	1.1907E+000	1.0000E+000	−1.1906E+000	+/−	0.0000E+000
4	1.7887E+000	1.0000E+000	−1.7887E+000	+/−	0.0000E+000
5	8.7890E+000	1.0000E+000	−8.7890E+000	+/−	0.0000E+000
6	1.3443E+001	1.0000E+000	−1.3443E+001	+/−	0.0000E+000
7	3.2186E+001	1.0000E+000	−3.2186E+001	+/−	0.0000E+000
8	1.5859E+002	1.0000E+000	−1.5859E+002	+/−	0.0000E+000
9	1.1541E+003	1.0000E+000	−1.1541E+003	+/−	0.0000E+000
10	5.2449E+004	1.0000E+000	−5.2449E+004	+/−	0.0000E+000
11	7.0687E+004	1.0000E+000	−7.0687E+004	+/−	0.0000E+000
12	2.3100E+005	1.0000E+000	−2.3100E+005	+/−	0.0000E+000
13	1.1919E+006	1.0000E+000	−1.1916E+006	+/−	0.0000E+000
14	1.8333E+006	1.0000E+000	−1.3330E+006	+/−	0.0000E+000
15	9.9012E+000	5.7900E−003	−5.7851E−002	+/−	9.9010E+000
16	2.6737E+001	1.4408E−002	−3.8525E−001	+/−	2.6734E+001
17	3.1066E+001	6.1722E−003	−1.9174E−001	+/−	3.1065E+001
18	4.6913E+001	6.5726E−003	−3.0834E−001	+/−	4.6912E+001
19	4.9364E+001	3.3015E−002	−1.6297E+000	+/−	4.9337E+001
20	8.5326E+001	1.2430E−003	−1.0606E−001	+/−	8.5326E+001
21	1.0733E+002	5.6653E−003	−6.0811E−001	+/−	1.0733E+002
22	1.5580E+002	5.9235E−002	−9.2292E+000	+/−	1.5553E+002
23	1.7399E+002	4.8493E−002	−8.4376E+000	+/−	1.7378E+002
24	1.8317E+002	6.3871E−003	−81.1699E+000	+/−	1.8316E+002
25	2.2741E+002	3.0828E−002	−87.0108E+000	+/−	2.2730E+002
26	2.4404E+002	1.2704E−002	−83.1005E+000	+/−	2.4402E+002
27	2.6391E+002	4.9231E−003	−81.2992E+000	+/−	2.6391E+002
28	2.8307E+002	5.1521E−002	−81.4584E+001	+/−	2.8270E+002
29	2.8673E+002	5.0303E−003	−81.4423E+000	+/−	2.8673E+002
30	3.1772E+002	2.3790E−002	−87.5589E+000	+/−	3.1763E+002
31	3.4643E+002	2.1642E−002	−87.4974E+000	+/−	3.4634E+002
32	3.9533E+002	1.5263E−002	−86.0342E+000	+/−	3.9528E+002
33	4.0819E+002	1.4912E−002	−86.0872E+000	+/−	4.0815E+002
34	4.1508E+002	1.2533E−002	−85.2025E+000	+/−	4.1505E+002
35	5.2271E+002	1.0400E−001	−85.4367E+001	+/−	5.198754E+002
⋮	⋮	⋮	⋮		⋮

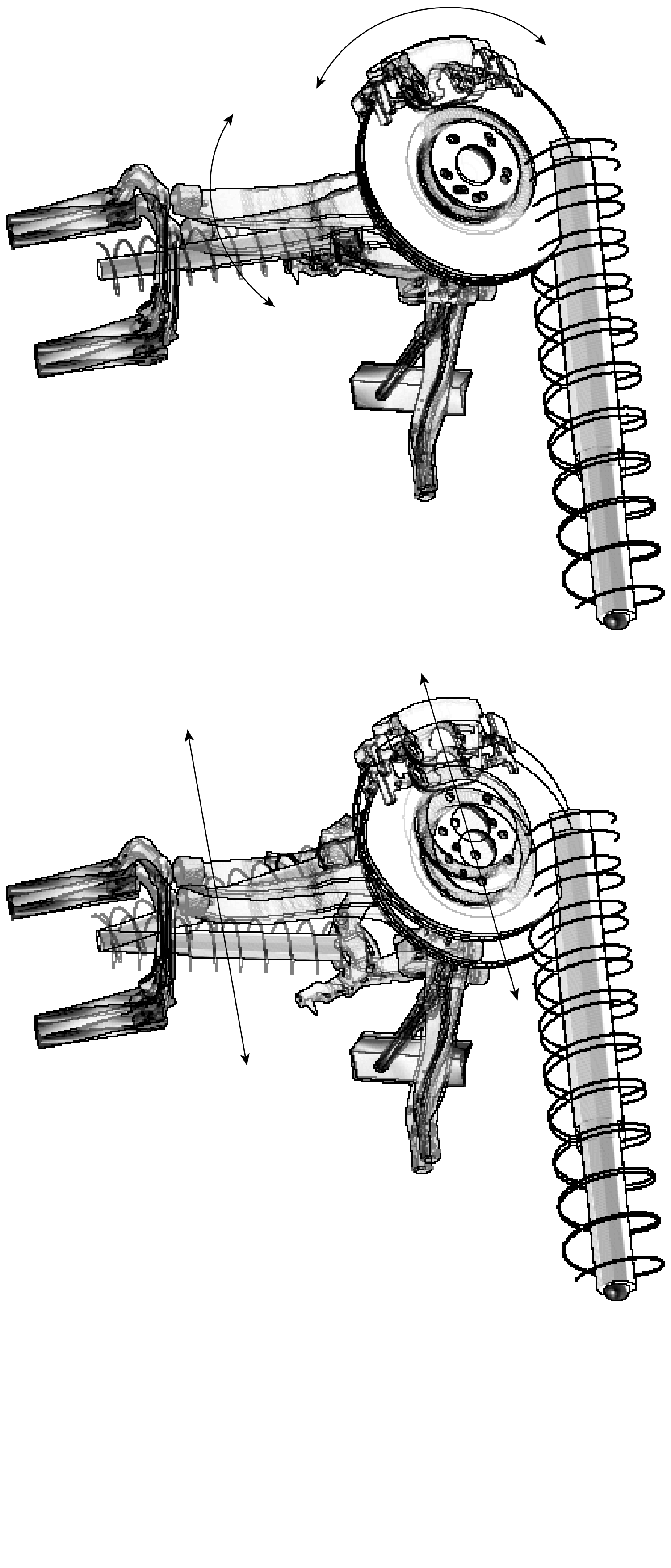

(a) 31 Hz, Mode 17

(b) 49 Hz, Mode 19

Figure 6.6: Equivalent modes to the primary modes found in the ODS analysis.

The first 35 stick modes of the ADAMS model are listed in Table 6.1 (note that mode numbers 1-15 are component rigid body modes and does not 'exist' in the numeric simulations). After the eigenvalues are produced, the shape of each suspect low frequency modes is animated and visually compared to the ODS results. With this method it could be found that the vibrations of ODS mode A is represented by ADAMS Mode number 17, and ODS mode B is represented by ADAMS Mode number 19.

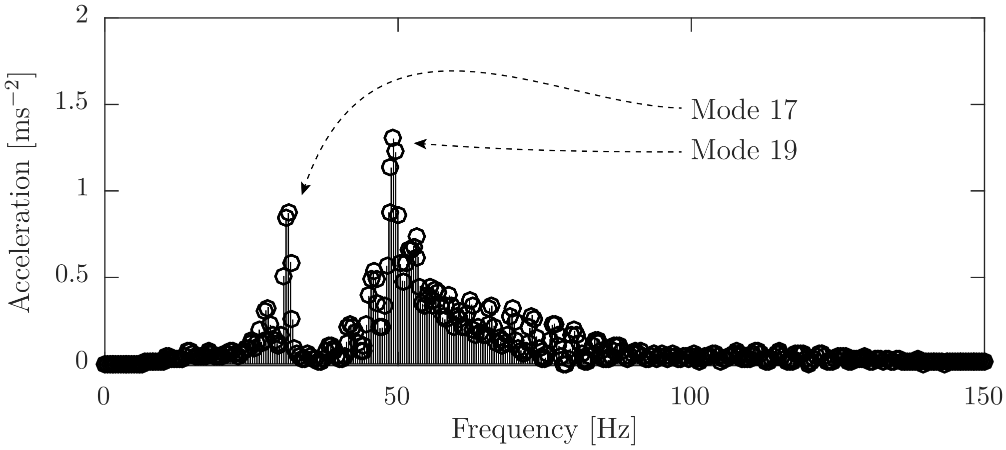

(a) ADAMS simulation

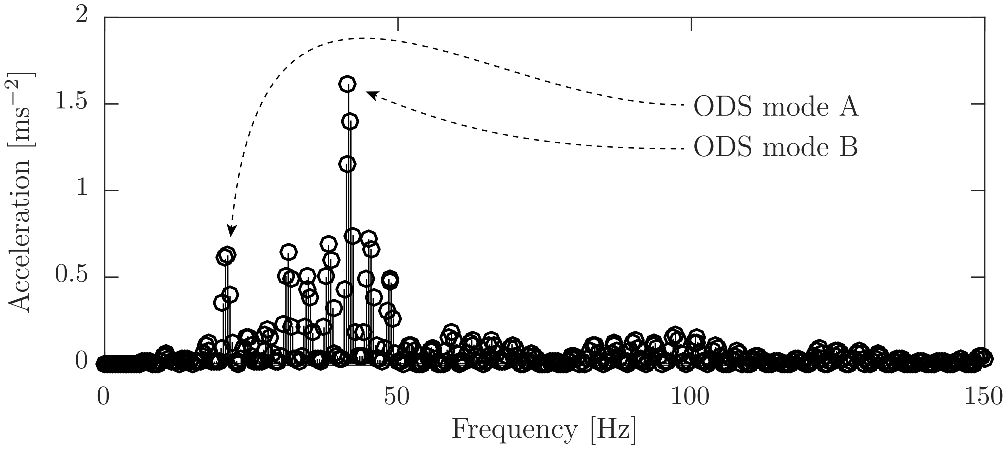

(b) Rig measurement

Figure 6.7: Caliper acceleration spectra (Z) of simulated and measured creep groan.

Studying the frequency content with knowledge of equivalent modes, it can be confirmed that model predictions comply with measurement results in terms of structural excitation.

6.3 Comments on calibration

Because reductions to geometry, the model is inherently limited in what it can represent and how accurate it can be. The initial simulations predicted relatively accurate results for stick-slip cycles, but the modes were skewed upward in frequency. This shift can be explained from the reductions on model geometry, for example how boundaries on `FLEX_BODY_CON_1` and `FLEX_BODY_CON_2` are fixated to inertial space as opposed to being attached to a softer frame, but also from the non-represented masses such as the ball bearings, bolts, brake fluids, etc. However, the initial bushing parameters are also expected to be incorrect as they are presumably estimated from a different load case. For this reason the model is primarily calibrated by modifying bushing parameters.

Bushing parameters affect both stick-slip cycles and modes, meaning if all bushings were lowered by some percentage it would correct the modes but disrupt the cycles. Thus, calibration proceeded with taking into consideration how different bushings contribute differently to stick-slip and/or primary modes *e.g.*, a stiffness change in `Bushing_3`'s Z-direction wouldn't affect stick-slip cycles or Mode 17 especially but will affect vibration frequency of Mode 19. The calibrated bushing parameters are found in Table 6.2.

Table 6.2: Calibrated bushing parameters

	Translational properties		Rotational properties	
	Stiffness [N/mm] (x,y,z)	Damping [Ns/mm] (x,y,z)	Stiffness [N/rad] (x,y,z)	Damping [Ns/rad] (x,y,z)
Bushing_1	(4000,4000,800)	(0.32,0.32,0.062)	(6000,6000,2000)	(0.001,0.001,0.001)
Bushing_2	(4000,4000,800)	(0.32,0.32,0.062)	(6000,6000,2000)	(0.001,0.001,0.001)
Bushing_3	(41000,32000,900)	(3.00,3.00,0.10)	(40000,40000,5000)	(0.001,0.001,0.001)
Bushing_4	(4100,600,300)	(0.3,0.075,0.02)	(4000,15000,4000)	(0.001,0.001,0.001)
Bushing_5	(34000,34000,2800)	(2.8,2.8,0.18)	(60000,60000,6000)	(0.001,0.001,0.001)

7

Discussion

The experimental measurement (or ADAMS model) does not attempt to recreate in-situ creep groan found in automotives, instead the thesis approaches creep groan from a phenomenological perspective. Meaning the created model cannot be applied directly for NVH verification 'as is', however it can be used to gain valuable understanding of creep groan through for example conducting a parametric study on the model.

All things considered the simulation offer strong qualitative and quantitative predictions of the measured 'pseudo-creep groan', though there are some potential shortcomings to acknowledge and discuss:

(A.) Several modes are unaccounted in the simulation, as evident when comparing Figure 6.7 (a) and (b). This may not seem as an issue as vibration patterns are usually regarded as orthogonal and decoupled from one another, however this does not hold for the type of bifurcating vibrations in creep groan (where the ODE or system equations are subject to change over time). It is speculated that stick-slip patterns in the rig are more irregular than in the simulation, but not by so much given the dominant primary modes.

(B.) The lack of representation in the model also causes it to be fundamentally stiffer and have less weight than its physical counterpart. It follows that all equivalent modes in the simulation should be of slightly higher eigenfrequency, but at the same time, various parameters are calibrated to make a more accurate simulation. Meaning there is a conflict where accurate frequencies corresponds to inaccurate parameter descriptions and vice versa.

(C.) The disc/pad contact force distribution during operation is expected to be hyperbolical[9] from 'wedging effects' as shown in Figure 7.1.

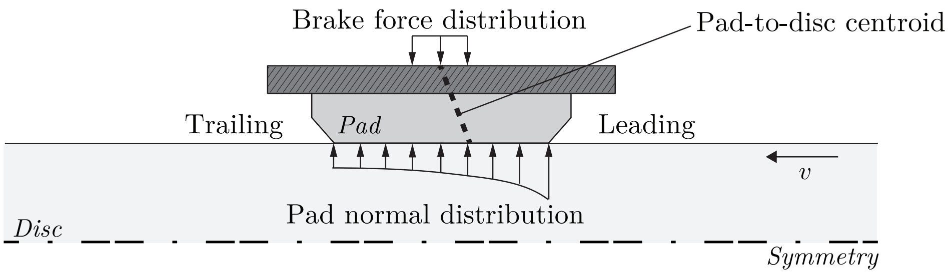

Figure 7.1: Illustration of nonlinear force distribution of pad/disc contact.

The nonlinear normal distribution means the interface centroid line is acutely angled toward the friction force which in turn constitute the basis for sprag-slip instability to occur[9],[11]. In theory, sprag event causes the friction force to grow significantly larger than what is predicted from the normal force due to geometric constraints[11]. In the model the brake pad surfaces are constrained to always be parallel in relation to one another; the normal distribution must be linear and the force centroid is thus perpendicular in relation to the contact. In other words, the model cannot accommodate sprag-slip dynamics. Note however that the calculated μ_s must contain influence from sprag (granted it occurred in the measurement), though the efficacy of describing sprag-slip using stick-slip is unknown.

(D.) The friction vs. relative velocity curve is modelled without path dependence, thus it does not correctly describe the slip-to-stick transition (*i.e.*, an increase in friction when transitioning from slip-to-stick is not reasonable).

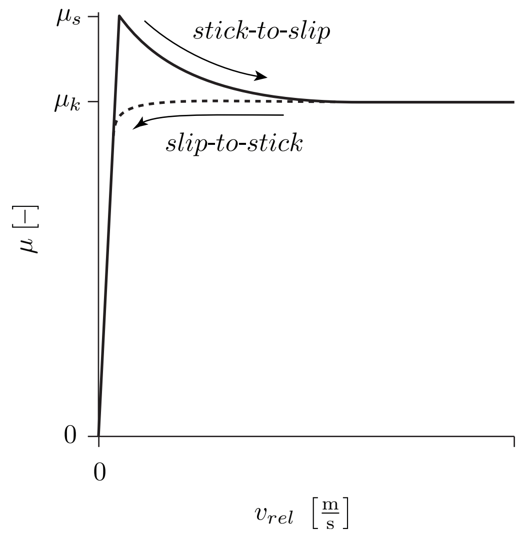

Figure 7.2: Example of nonholonomic v_{rel} constraint on friction.

It has been shown in a previous study that a path independent friction model 'predicts a sharp spike in acceleration at the onset of stick'[10] that was unaccounted for in their test data. Such spikes should reasonably also be observed in Figure 6.2 (a), but on the contrary it appears that the rig measurement has sharper acceleration spikes on stick transitions. This is possibly explained by re-stick incidentally occurring at greater speeds in the measurement and/or sprag-slip phenomena.

8

Conclusions

With a combination of rigid and flexible bodies, a multi-body model was developed in ADAMS to reproduce measured creep groan dynamics developed in an experimental rig. The rig measurements were conducted in a laboratory environment which, in addition to vibration behaviour, also allowed for the retrieval of various operation parameters and values that was implemented in the design process and considered in evaluation.

From analysing numeric and analytic solutions of the model and comparing them to the experimental results it could be demonstrated that the simulated predictions are largely consistent with the measured vibrations in terms of stick-slip dynamics, frequency content and vibration patterns. And in the broader perspective, the thesis work has been able present effective methods for theoretically deconstructing, experimentally recreating and finally achieving qualitatively, as well as quantitatively accurate simulations of creep groan phenomena using CAE software(s).

Bibliography

[1] J. Yoon A. R. Crowther and R. Singh. "An Explanation for Brake Groan Based on Coupled Brake-Driveline System Analysis". In: SAE International (2007).

[2] About Adams/Solver 2015. MSC Software.

[3] A. Akay. "Acoustics of friction". In: Acoustical Society of America (2001).

[4] G. Amontons. "De la résistance causée dans les machines". In: Mém. Acad. Sci. (1699).

[5] C.C. de Wit B. Armstrong. Friction Modeling and Compensation. CRC Press, 1995.

[6] M. T. Bengisu and A. Akay. "Stability of friction-induced vibrations in multi-degree-of-freedom systems". In: Journal of Sound and Vibration (1994).

[7] E.J. Berger. "Friction modeling for dynamic system simulation". In: App. Mech. Rev. (2002).

[8] C.A. Coulomb. "Théorié des Machines simples". In: Mém. Math. Phys. Acad. Sci. (1781).

[9] Y. Dai and T. C. Lim. "Suppression of brake squeal noise applying finite element brake and pad model enhanced by spectral-based assurance criteria". In: Applied Acoustics (2008).

[10] M. Donley and D. Riesland. "Brake Groan Simulation for a McPherson Strut Type Suspension". In: SAE International (2003).

[11] Handbook of Friction-Vibration Interactions, 1st Edition. G. Chen, 2014.

[12] W. Kropp. Propagation and radiation of structure borne sound. 2015.

[13] M. Oestreich N. Hinrichs and K. Popp. "On the modeling of friction oscillators". In: Journal of Sound and Vibration (1998).

[14] A. De Kraker R. I. Leine D. H. Van Campen and L. Van den Steen. "Stick-Slip Vibrations Induced by Alternate Friction Models". In: Kluwer Academic Publishers (1998).

[15] S.H. Kim H. Jang M.Y. Cho W.K. Lee M.W. Shin. "The influence of humidity on the sliding friction of brake friction material". In: Wear (2013).

A

MDOF stick-slip model

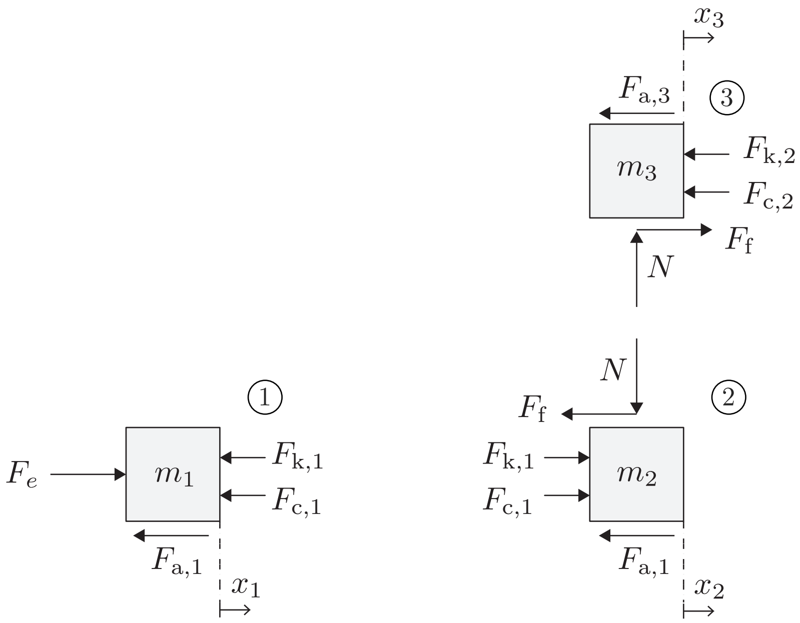

Figure A.1: Active-force diagram of Figure 2.5.

Separating the forces in Figure A.1 (with $F_{\mathrm{k,n}} = k_{\mathrm{i}}\Delta x$, $F_{\mathrm{c,n}} = c_{\mathrm{i}}\Delta\dot{x}$, $F_{\mathrm{a,n}} = m_{\mathrm{n}}\ddot{x}_{\mathrm{n}}$, $F_{\mathrm{f}} = \mu(v_{\mathrm{rel}})N$ and $v_{\mathrm{rel}} = \dot{x}_2 - \dot{x}_3$):

$$\begin{aligned} ①\rightarrow: 0 &= F_e - F_{\mathrm{k},1} - F_{\mathrm{c},1} - F_{\mathrm{a},1} \\ &\Rightarrow -F_e = -k_1(x_1 - x_2) - c_1(\dot{x}_1 - \dot{x}_2) - m_1\ddot{x}_1 \end{aligned} \tag{A.1}$$

$$\begin{aligned} ②\rightarrow: 0 &= \; - F_{\mathrm{f}} + F_{\mathrm{k},1} + F_{\mathrm{c},1} - F_{\mathrm{a},2} \\ &\Rightarrow \mu(v_{\mathrm{rel}})N = k_1(x_1 - x_2) + c_1(\dot{x}_1 - \dot{x}_2) - m_2\ddot{x}_2 \end{aligned} \tag{A.2}$$

$$\begin{aligned} ③\rightarrow: 0 &= F_{\mathrm{f}} - F_{\mathrm{k},2} - F_{\mathrm{c},2} - F_{\mathrm{a},3} \\ &\Rightarrow -\mu(v_{\mathrm{rel}})N = -k_2x_3 - c_2\dot{x}_3 - m_3\ddot{x}_3 \end{aligned} \tag{A.3}$$

Combined, the equations (A.1),(A.2) and (A.3) comprise the system equation of motion (written as general system form in Equation (2.8)).

B

MDOF stick-slip model (MATLAB)

Main

```
% Vars
global m1 m2 m3 k1 k3 c1 c3 N alfa beta fr mag epsi

% Parameter initialize
m1 = 200;                              % Mass [kg]
m2 = (2.56615*10^5)/(140.1540^2);      % -
m3 = 9.7898;                           % -
k1 = (5E+005)/1000/0.017/(0.14^2);     % Stiffness [Nm]
k3 = (3000)*1000;                      % -
c1=(50)/1000/0.0174/(0.14^2);          % Damping [Nm/s]
c3=(5.0E-002)*1000;                    % -
N = 7200;                              % Normal [N]
alfa=50;
beta=1000;
fr=1.2500;
mag=0.402;
epsi=100;

%% Solve Non-linear stiff ODE
cond = zeros(1,6);                     % IC
tspan = linspace(0,1,100000);
opts=odeset('RelTol',1.e-7,'AbsTol',1.e-10);

[t,Z] = ode15s('xprim3_3m',tspan,cond,opts);

%% Plots
...
```

ODE call function

```
function Zp = xprim3_3m(t,Z)

% Vars
global m1 m2 m3 k1 k3 c1 c3 N alfa beta fr mag epsi
```

```

vrel = Z(5)-Z(6);

Q1=1-exp(-beta*abs(epsi*vrel));
Q2=1+(fr-1)*exp(-alfa*abs(epsi*vrel));
Q3=sign(epsi*vrel);
u=mag*Q1*Q2*Q3;

Ff = u*N;
Fe = 4310*(sin(2*pi*t/1).*(t<0.25)+(t>=0.25));
FF = [-Fe, Ff, -Ff, 0, 0, 0]';
KK = [  -k1,    +k1,    0;
        +k1,    -k1,    0;
         0,      0,    -k3];
CC = [  -c1,    +c1,    0;
        +c1,    -c1,    0;
         0,      0,    -c3];
MM = [  -m1,     0,     0;
         0,     -m2,    0;
         0,      0,    -m3];
AA = [KK,CC;zeros(3,3),diag(ones(1,3))];
BB = [zeros(3,3),MM;-diag(ones(1,3)),zeros(3,3)];
Zp = BB\(FF-AA*Z);
```

C

ODS Analyser (MATLAB)

Main

```
%  Aquire signals and coordinates
dataFilepath = 'Acceleration.txt';
aar = dlmread(dataFilepath);

sysFilepath = 'Coordinates for ODS.xls';
[val,~,~] = xlsread(sysFilepath);
val(isnan(val)) = 0;

fs = 12500;        % Sample rate [Hz]
t1 = 4;            % Sample start [s]
t2 = 5.8;          % Sample end [s]
fchosen = 25;      % Frequency of interest [Hz]
s = 12;            % Scaling factor [dimless]
tsc = 1;           % Time scaling factor [dimless]
drawNum = 1;       % Draw numbers
drawLine = 1;      % Draw lines

% Calculate
aar = aar(:,1:24);
[norg,~] = size(aar); % n for number of samples

dt = 1/fs;
tr = (0:norg-1)*dt; % Time vector

% Define time matrix
ti=intersect(find(tr>t1),find(tr<t2));     % Timeframe index
t = tr(ti);

aa = aar(ti,:);
[n,k] = size(aa);

% Hanning window
Hw = hanning(n);                           % Window function
```

```
Hwsc = sqrt(sum(Hw.^2)/length(Hw)); % Window scaling

% Filter specification
fmin = 20;         % HP cutoff frequency
fmax = 4000;       % LP cutoff frequency
bpSpec = fdesign.bandpass('N,F3dB1,F3dB2',8,fmin,fmax,fs);
bp = design(bpSpec,'butter');

% Adoptize and fourier transform acceleration matrix
nFFT = 2^nextpow2(n);
f = fs/2*linspace(0,1,nFFT/2);
for i = 1:k
    yhw = aa(:,i).*Hw/Hwsc;        % Apply window
    yfhw = filter(bp,yhw);         % Apply filter
    Yds = fft(yfhw,nFFT)/10;       % Take FFT, normalize
    AA(:,i) = 2*Yds(1:nFFT/2);    % Reshape & rescale
end

an=1;

% Accelerometer local coordinate system
v = val(2:end,5);
AAdir = vec2mat(v,3);
AAorg = vec2mat(AA(find(f > fchosen,1),:),3);
for i = 1:8
    v = [AAdir(i,:)',AAorg(i,:)'];                   % Def. vec.
    v(:,2) = v(:,2).*(v(:,1))./abs((v(:,1)));    % Adjust dir.
    v = sortrows(v,abs(1));                          % Sort vec.
    AAs(i,:) = [v(:,2)]';                            % Restore
end

Ax = AAs(:,1);
Ay = AAs(:,2);
Az = AAs(:,3);

w=2*pi*fchosen; % Angular frequency

% Displacements
for i = 1:length(Ax);
    ux(i,:) = real(Ax(i)*exp(1j*w*t)/(1j*w)^2)*s;
    uy(i,:) = real(Ay(i)*exp(1j*w*t)/(1j*w)^2)*s;
    uz(i,:) = real(Az(i)*exp(1j*w*t)/(1j*w)^2)*s;
end

% Global coordinate system
na = 8;
```

```
for i_1 = 1:na
    coords(i_1,:) = val(2+(3*(i_1-1)),6:8)*1e-3;
end

lx = repmat(coords(:,1),1,n)+ux;
ly = repmat(coords(:,2),1,n)+uy;
lz = repmat(coords(:,3),1,n)+uz;


% Accelerometer displacement
figure(4)
set(4, 'units', 'pixels', 'pos', [0 0 426 426]*3/2)
%title(['Accelerometer positions at ' num2str(fchosen) ...
%     ' Hz (with upscaled deformations).'])
xlabel('x [m]'), ylabel('y [m]'), zlabel('z [m]')
%
grid on
hold on
axis ([1.3 1.8 0.4 1 0.2 1])
daspect([1 1 1])

for i_3 = 1:1
    %set(gca,'NextPlot','replaceChildren');
    for i_9 = 1:8
        plot3(lx(i_9,i_3),ly(i_9,i_3),lz(i_9,i_3), ...
                'or','Markersize',4, 'MarkerFaceColor', ...
                'k','Color','k')
        if drawNum == 0
            text(lx(i_9,i_3)-0.02,ly(i_9,i_3),lz(i_9,i_3) ...
                +0.02, num2str(i_9), 'Color', 'k');
        end
        if drawLine == 1
            line([lx(1:2,i_3)],[ly(1:2,i_3)], ...
                [lz(1:2,i_3)],'Color', [0.5 0.5 0.5])
            line([lx([4 3],i_3)],[ly([4 3],i_3)], ...
                [lz([4 3],i_3)],'Color', [0.5 0.5 0.5])
            line([lx([5 6],i_3)],[ly([5 6],i_3)], ...
                [lz([5 6],i_3)],'Color', [0.5 0.5 0.5])
            line([lx(7:8,i_3)],[ly(7:8,i_3)], ...
                [lz(7:8,i_3)],'Color', [0.5 0.5 0.5])
        end
        hold on
    end
    view([172,8])
    %pause(dt*tsc)
    %mov(i_3) = getframe(gcf, [0 0 1120 840]);
```

```
end

%movie2avi(mov, 'Anim.avi');
camproj('perspective')

% Plots
...
```